

AN EVALUATION OF THE CORROSION RESISTANCE  
OF 2 1/4 Cr - 1 Mo STEEL  
IN A LITHIUM-LEAD LIQUID

By

Ted L. Anderson

Colorado School of Mines

1964  
COLORADO SCHOOL OF MINES LIBRARY

ProQuest Number: 10782194

All rights reserved

INFORMATION TO ALL USERS

The quality of this reproduction is dependent upon the quality of the copy submitted.

In the unlikely event that the author did not send a complete manuscript and there are missing pages, these will be noted. Also, if material had to be removed, a note will indicate the deletion.



ProQuest 10782194

Published by ProQuest LLC (2018). Copyright of the Dissertation is held by the Author.

All rights reserved.

This work is protected against unauthorized copying under Title 17, United States Code  
Microform Edition © ProQuest LLC.

ProQuest LLC.  
789 East Eisenhower Parkway  
P.O. Box 1346  
Ann Arbor, MI 48106 – 1346

SUBMITTAL SHEET

A thesis **sub**mitted to the Faculty and the Board of Trustees of the Colorado School of Mines in partial fulfillment of the requirements for the degree of Master of Science (Metallurgy).

Signed: Ted L. Anderson  
Student

Date: 7/1/80

Approved: Alan Edwards  
Thesis Advisor

W. D. [Signature]  
Head of Department

Date: July 8, 1980

ABSTRACT

Significant penetration at prior austenitic grain boundaries was observed in the heat-affected zones of GTA-welded 2 1/4 Cr - 1 Mo steel after the metal was exposed at 500C for short times to liquid lithium containing 17.6 wt% lead. This HAZ attack was anticipated since thermodynamic data indicate that cementite is unstable in lithium at 500C. The intergranular attack has been studied with respect to microstructural changes resulting from the welding process. Corrosion resistance was greatly improved in weldments which were given a post-weld heat treatment to convert cementite to  $M_{23}C_6$  and/or  $M_6C$ . It was also found that niobium-stabilized 2 1/4 Cr - 1 Mo steel was resistant to intergranular attack, even when no post-weld heat treatment was applied.

To prepare larger, microstructurally homogeneous but corrosion-susceptible specimens for detailed study, coupons of 2 1/4 Cr - 1 Mo steel were heat treated so as to simulate the coarse-grained bainitic microstructures found in the heat affected zones of GTA weldments. The coupons were exposed to Li-17.6% Pb at various temperatures.

Lithium corrosion was found to increase with increasing austenitizing temperature and to be insensitive to quench

rate. The penetration vs time<sup>1/2</sup> curves for the corrosion-susceptible microstructures exhibited a change in slope which is hypothesized to be associated with the conversion of  $\epsilon$ -carbide to cementite. The initial corrosion rate has an activation energy of 5.3 kcal/mole and is thought to be controlled by carbon diffusion in lithium. The secondary corrosion rate, which has an activation energy of 28 kcal/mole, is probably reaction controlled.

## TABLE OF CONTENTS

	Page
INTRODUCTION . . . . .	1
Previous Lithium Corrosion Studies. . . . .	2
The Physical Metallurgy of 2 1/4 Cr - 1 Mo Steel. . .	4
1. Applications and Specifications. . . . .	5
2. Microstructure and Heat Treatment. . . . .	6
3. Welding Metallurgy . . . . .	14
4. Carbide Stability in Lithium . . . . .	14
Experimental Scope. . . . .	15
EXPERIMENTAL PROCEDURE . . . . .	18
Corrosion of GTA Weldments. . . . .	18
Corrosion of Simulated Weldments. . . . .	25
Stress Tests. . . . .	26
RESULTS AND DISCUSSION . . . . .	27
Corrosion of GTA Weldments. . . . .	27
Corrosion of Simulated Weldments. . . . .	41
1. Initial Corrosion. . . . .	52
2. Secondary Corrosion. . . . .	56
Auger Spectroscopy. . . . .	59
Weight Loss . . . . .	62
Stress Effects. . . . .	63
SUMMARY AND CONCLUSIONS. . . . .	65
REFERENCES . . . . .	67

LIST OF FIGURES

<u>Figure</u>		<u>Page</u>
1	The continuous cooling diagram for 2 1/4 Cr - 1 Mo steel.	7
2	Carbide stability diagrams for quenched and tempered and normalized and tempered 2 1/4 Cr - 1 Mo steel.	11
3	Relative thermodynamic stability of several carbides in carbon saturated lithium.	16
4	Schematic of a GTA-welded coupon.	19
5	Schematic drawing of apparatus used in weight loss and penetration studies.	22
6	Lithium sampling device.	24
7	Intergranular penetration of a 2 1/4 Cr - 1 Mo (regular grade) GTA weldment at prior austenitic grain boundaries in the heat-affected zone.	28
8	A regular grade GTA weldment (10 hrs at 760C post-weld H.T.) exposed to lithium-17.6 w/o lead at 500C.	29
9	Nb-stabilized GTA weldment (no post-weld H.T.) exposed to lithium-17.6 w/o lead at 500C.	30
10	Effect of post-weld heat treatment on the corrosion of GTA heat-affected zones.	31
11	Penetration vs. time <sup>1/2</sup> as a function of post-weld heat treatment and niobium content of GTA weldments exposed to Li-17.6% Pb at 500C.	33
12	Corrosion of the Nb-stabilized 2 1/4 Cr - 1 Mo parent metal.	34

<u>Figure</u>		<u>Page</u>
13	"Wormhole" attack of the post-weld heat treated heat-affected zones.	36
14	SEM micrographs of HAZ corrosion of a post-weld heat treated weldment.	37
15	Carbides formed during the tempering of quenched 2 1/4 Cr - 1 Mo steel.	39
16	Comparison of microstructure from the heat-affect zone of an actual GTA weldment and a specimen heat treated to simulate the HAZ microstructure.	42
17	Intergranular penetration of a simulated HAZ specimen after 1 hour of exposure to Li-17.6% Pb at 500C.	43
18	Intergranular penetration of 2 1/4 Cr - 1 Mo steel simulated weldments in Li-17.6% Pb at 500C.	44
19	Corrosion of simulated weldments as a function of time <sup>1/2</sup> and test temperature.	47
20	Comparison of the change in corrosion rate with the conversion of epsilon carbide to cementite in quenched 2 1/4 Cr - 1 Mo steel.	49
21	Arrhenius plot of the corrosion rate constant as a function of temperature for simulated weldments.	51
22	Photomicrographs of the corrosion of a simulated weldment during the initial corrosion mechanism.	53
23	Schematic of a corroded grain boundary during the initial corrosion mechanism.	55
24	Decarburization of a simulated weldment during secondary corrosion.	57

<u>Figure</u>		<u>Page</u>
25	Comparison of the uncorroded microstructure and the matrix decarburized during secondary corrosion.	58
26	Schematic of a corroded grain boundary during the secondary corrosion mechanism.	60
27	Auger spectra of three regions of a GTA weldment fractured along a corroded grain boundary.	61

LIST OF TABLES

<u>Table</u>		<u>Page</u>
I	Chemical compositions of the two alloys used in this investigation.	18
II	Data matrix for the GTA weldment corrosion study.	20

ACKNOWLEDGEMENTS

I would like to express my deepest appreciation to the members of my thesis committee, Drs. G.R. Edwards, D.L. Olson and D.K. Matlock. I especially thank Dr. Edwards for the guidance he has given me these past two years. The assistance of the following people is gratefully acknowledged. Richard McNealy performed some of the initial experimental work which appears in this thesis. Dr. Jessie Lumsden of Rockwell International performed the Auger spectroscopy shown in Figure 27. Many of the drawings which appear in this thesis were prepared by Bruce Wilkinson. Dr. Nate Hoffman of Rockwell International, who has continuously shared his expertise and has given us a great deal of helpful advise, is also deserving of our deepest gratitude.

This research was funded by the Lawrence Livermore Laboratories and the National Association of Corrosion Engineers.

## INTRODUCTION

The unique chemical, physical and nuclear properties of lithium make it attractive for a number of potential applications. Among these is inertial confinement fusion reactors, where a liquid lithium blanket would protect the main reactor wall from neutron damage, act as a coolant, and simultaneously create new fuel as neutrons convert lithium to tritium. A major drawback of lithium is its corrosive nature.

Engineering alloys for lithium containment in a fusion reactor must meet criteria of availability, fabricability and code acceptance in addition to being acceptably resistant to liquid lithium corrosion. The major potential candidates have traditionally been 304 stainless steel and 2 1/4 Cr - 1 Mo steel (either regular grade or Nb-stabilized). Data generated by the Colorado School of Mines(1) indicate that both alloys have good resistance to liquid lithium attack. However, cost and availability of 304 stainless steel make it less desirable than 2 1/4 Cr - 1 Mo steel. An additional consideration is that relatively long-lived radioactive isotopes are produced in 304 stainless steel when nickel atoms in the alloy are subjected to a high

neutron flux. The pressure vessel steel, 2 1/4 Cr - 1 Mo, is presently the most viable candidate for lithium containment. A detailed analysis of the corrosion of this steel by lithium has become necessary and timely.

### Previous Lithium Corrosion Studies

Liquid lithium corrosion of pure metals was initially studied by a number of investigators(2-6) to obtain relative corrosion resistance data for material selection. Failure to recognize the importance of impurity contamination and dissimilar-metal transfer effects resulted in a great deal of scatter and contradiction in the early results.

The principle factors affecting the severity of corrosion attack have been found to be temperature, temperature gradient, cyclic temperature fluctuation, ratio of material area to lithium volume, impurity level in the lithium, flow velocity, the material's surface condition, the number of solid materials in contact with the lithium, and the metallurgical condition of the container material. More complete discussions of these mechanisms and controlling factors may be found in other references(2, 7-10). Lithium corrosion tests have been performed on large number of metals and alloys in the past 30 years. The major results of this work are summarized briefly below.

Pure iron is highly resistant to lithium corrosion below  $\sim 1000^{\circ}\text{C}$ (2,11,12). Lithium attack is greatly accelerated if the iron is stressed(11,13). The corrosion resistance of iron decreases with increasing carbon content because  $\text{Fe}_3\text{C}$  can be reduced to form  $\text{Li}_2\text{C}_2$ (14).

Austenitic stainless steels are subject to preferential leaching, resulting in a ferritic surface layer (2,4,15-19). The rate of lithium attack of stainless steel increases with increasing nitrogen content in the lithium(9,20-24). If chromium carbides form at the grain boundaries, the surrounding chromium depleted region is subject to nickel leaching(25,26).

Nickel- and cobalt-base alloys have poor lithium corrosion resistance because of the high solubilities of cobalt and nickel in liquid lithium(2,27). These alloys have experienced intergranular attack(22,28,29) and selective leaching(7).

The refractory metals and alloys generally have excellent corrosion resistance in lithium. Molybdenum and its alloys give good service at elevated temperatures, even in the presence of nitrogen and oxygen contaminations(5,7,8,30,31). Niobium and tantalum have good lithium corrosion resistance, but are subject to attack in the presence of oxygen.

Very little research has been performed evaluating the lithium corrosion resistance of carbon steels. In general, any steel having significant amounts of  $Fe_3C$  will have unsatisfactory corrosion resistance. Beskorovainyi, et al.(14,32) performed preliminary evaluations on plain carbon steel, and Selle(15) presented data which indicated that 2 1/4 Cr - 1 Mo steel was resistant to lithium corrosion when the nitrogen concentrations in the lithium were low. More recent data show that heat affected zones of 2 1/4 Cr - 1 Mo weldments are susceptible to intergranular attack(1). There is evidence which suggests that lithium can adversely affect mechanical properties of steel. Matlock et al.(33) observed an increase in the rate of fatigue crack propagation in 2 1/4 Cr - 1 Mo steel and 304 L stainless steel in the presence of liquid lithium.

#### The Physical Metallurgy of 2 1/4 Cr - 1 Mo Steel

Steel of the nominal composition 2 1/4 Cr - 1 Mo has a long history of successful application in heavy structure operating at moderate temperatures. The steel is supplied under many different specifications according to application and has a complex carbide metallurgy. For that reason, a brief description of specifications and typical applications as well as a summary of the major metallurgical features is

included in this thesis to prepare the reader for a study of the material's lithium corrosion resistance.

1. Applications and Specifications: 2 1/4 Cr - 1 Mo steel is commonly used in applications such as hydrocarbon processing plants and the steam generators of Liquid Metal Fast Breeder Reactors (LMBR). The alloy was originally developed for service at elevated temperatures, where resistance to creep is the primary consideration, and it is widely used for steam boiler tubes and other parts operating in the 540C to 595C (1000F to 1100F) range.

2 1/4 Cr - 1 Mo steel is currently seeing widespread use in the demanding applications of reactors and pressure vessels for new processing operations such as coal gasification and liquefaction. These applications require the increased strength, creep resistance, oxidation resistance and corrosion resistance that this alloy offers over plain carbon steels(34).

2 1/4 Cr - 1 Mo is available under ASTM specifications A213, Grade T22, for tubing; A336, Grade F22, for drum forgings; A335, Grade P22, for pipe; A356, Grade 10 and A217, Grade WC9, for castings; A387, Grade D and A542, for plate. The A387D specification includes Class I (60-85 ksi tensile strength). The Class I heat treatment is usually an anneal, while Class II requires normalizing and tempering.

The higher strength versions of 2 1/4 Cr - 1 Mo plate are covered by A542. The properties of this specification are obtained by quenching and tempering; the tensile strengths of the four classes within the A542 specification range from 85 to 125 ksi.

## 2. Microstructure and Heat Treatment:

a. Austenitizing: The continuous cooling transformation (CCT) diagram for 2 1/4 Cr - 1 Mo steel is shown in Figure 1(35). Austenitizing of the alloy is usually accomplished in the 950C to 1000C temperature range. Normal commercial heat treatment practice results in one of three different conditions after austenitizing: annealed, normalized or quenched.

The annealed structure results from slow cooling (usually furnace cooling) from the austenitizing temperature and consists of proeutectoid ferrite with typically about 20% upper bainite. The upper bainite in the annealed structure has a lamellar appearance similar to pearlite.

A somewhat faster cooling rate, on the order of 300C/hr, results in a normalized structure, which contains both proeutectoid ferrite and bainite. The resulting bainite contains both plate-like and lath-like carbides in a Widmanstatten pattern. The

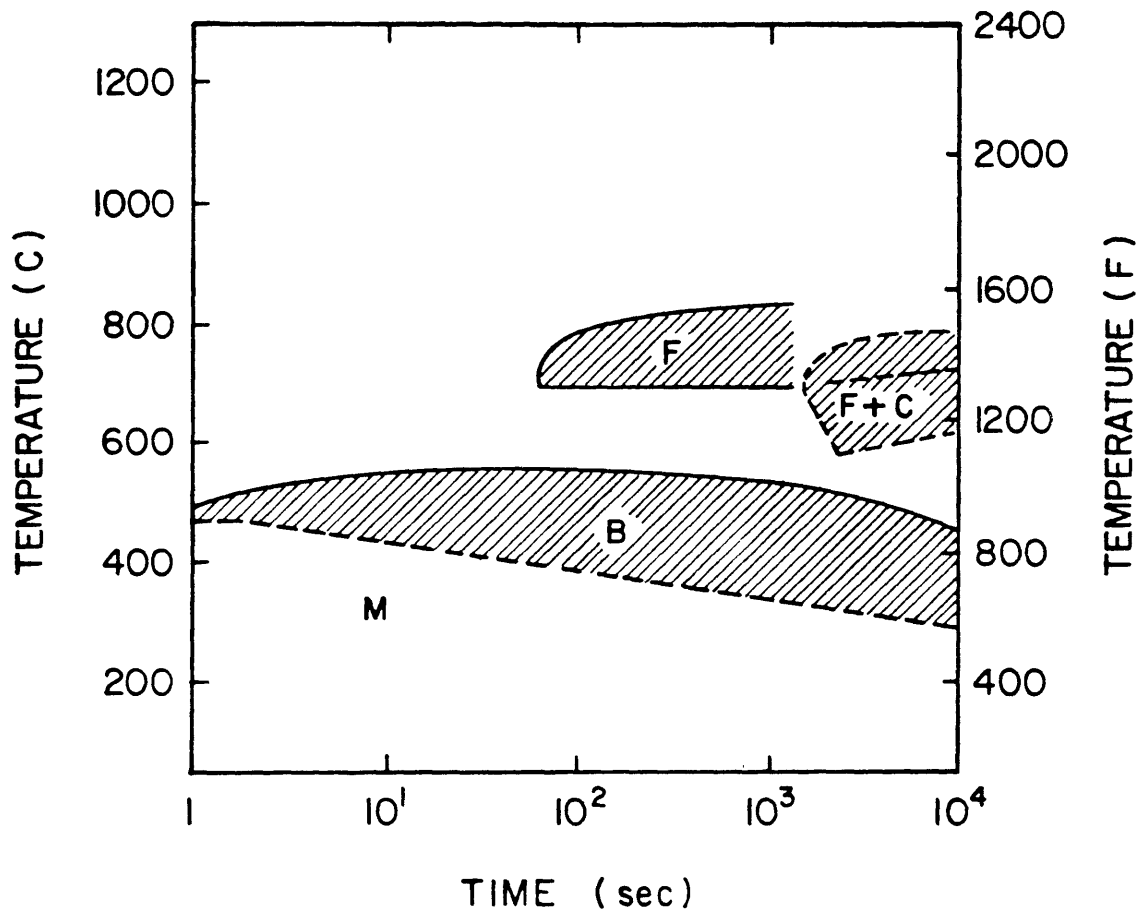


Figure 1. The continuous cooling diagram for 2 $\frac{1}{4}$ Cr-1Mo steel(35)

precipitates are mainly  $\epsilon$ -carbide with some cementite. Although  $\epsilon$ -carbide is generally thought to be exclusively a martensitic transformation product, several investigators(36,37) have observed  $\epsilon$ -carbide precipitation in bainite in Cr-Mo steels. In addition, there is some evidence that a small amount of acicular  $\text{Mo}_2\text{C}$  exists in the normalized structure on the ferrite side of the ferrite-bainite boundaries(37,38).

Quenching 2 1/4 Cr - 1 Mo steel yields a microstructure of acicular auto-tempered martensite and lower bainite with plate-like precipitates of  $\epsilon$ -carbide(37). Some grains also contain large lenticular plates of cementite. It is possible during quenching to obtain some minor constituents such as retained austenite or proeutectoid ferrite, depending in the quenching conditions and section thickness.

As can be seen from the foregoing discussion 2 1/4 Cr - 1 Mo does not possess a high degree of hardenability, as it is very difficult to obtain a totally martensitic microstructure. On the other hand, unlike most carbon and low alloy steels, it is also very difficult to form pearlite. Therefore the structure of 2 1/4 Cr - 1 Mo is typically a combination of proeutectoid ferrite and bainite, with the relative

amounts of each dependent of the rate of cooling from the austenitizing temperature.

Because of the relatively low hardenability of 2 1/4 Cr - 1 Mo steel, heavy sections are usually supplied in the annealed condition. In an effort to improve the hardenability of this steel (so that heavier section thicknesses could be heat treated to higher strength levels) Copeland and Pense(39) have studied the effect of varied carbon, nickel and aluminum contents on hardenability. They found that maintaining the carbon and alloying elements at high levels suppressed the formation of low strength polygonal ferrite. They were also able to predict the strength of tempered 2 1/4 Cr - 1 Mo by knowing the ferrite content and tempering temperature.

After 2 1/4 Cr - 1 Mo steel has been austenitized and cooled to ambient temperature the carbides reside almost exclusively in the bainite and/or autotempered martensite. The proeutectoid ferrite contains almost no carbides and is strengthened solely by the solid solution strengthening of alloying elements.

b. Tempering: 2 1/4 Cr - 1 Mo steel can be tempered from either the quenched or normalized conditions.

Tempering consists of a series of carbide precipitation

and transformation reactions. These reactions have been investigated by Baker and Nutting(37) in a systematic study of the carbides present after tempering at different temperatures for various times. The carbides were evaluated using optical metallography, electron microscopy, electron diffraction, x-ray diffraction and x-ray fluorescence.

One of the significant results of this study is shown in Figure 2, where the sequence of carbide formation during tempering can be seen for both the quenched and normalized conditions. The precipitation reactions and kinetics are similar for both conditions, apparently because the tempering characteristics of bainite and martensite are similar in this alloy. The differences lie in the morphology of the precipitated carbides.

As discussed previously, the normalized microstructure contains a substantial amount of proeutectoid ferrite. This is why  $\text{Mo}_2\text{C}$  precipitates more readily in this structure. Most of the carbides formed during tempering tend to nucleate on previous carbides within the bainitic structure; however  $\text{Mo}_2\text{C}$  nucleates within the ferrite matrix. In quenched 2 1/4 Cr - 1 Mo steel this nucleation occurs in the ferrite

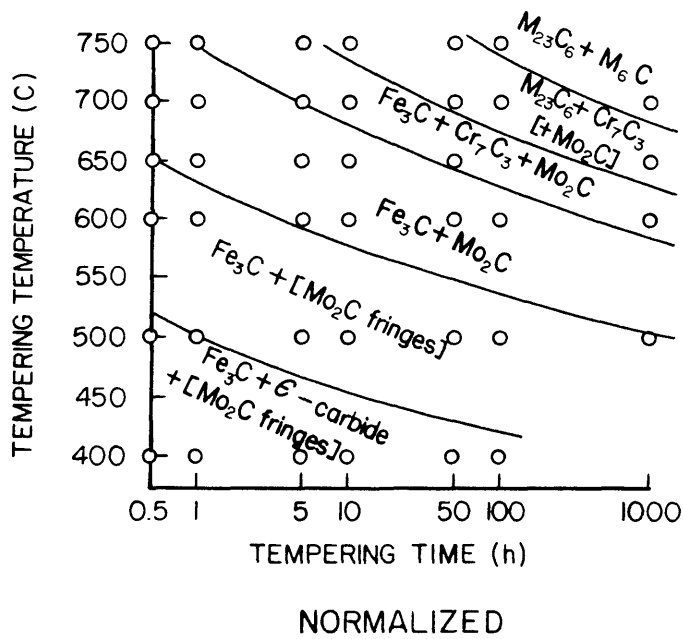
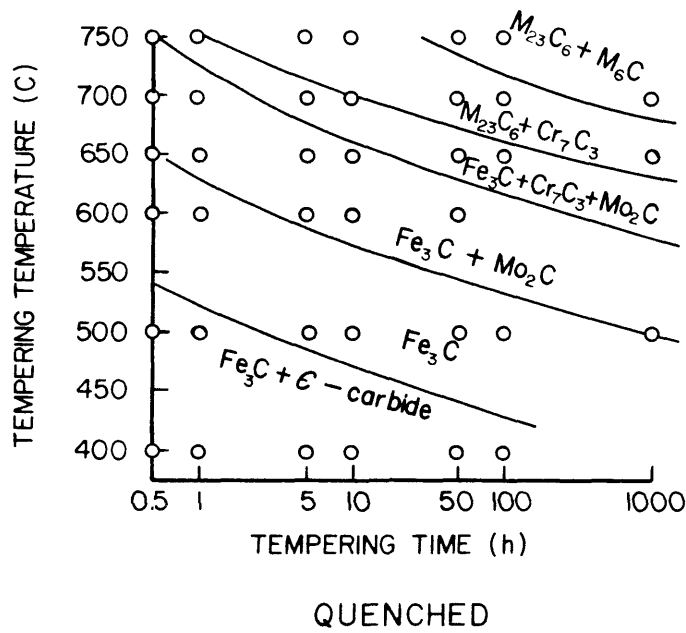
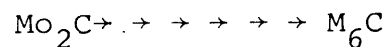


Figure 2. Carbide stability diagrams for quenched and tempered and normalized and tempered 2 1/4 Cr - 1 Mo steel(37).



## (ii) Ferrite



Epsilon carbide is present in ferrite laths in both normalized and quenched 2 1/4 Cr - 1 Mo.  $\epsilon$ -carbide and cementite precipitate on grain boundaries when the steel is tempered for short times at 400C.  $\epsilon$ -carbide does not completely transform to cementite until after about 5 hours at 500C. As this transformation occurs, the carbide plates become thicker and the iron is partially replaced in the cementite by chromium and manganese. Upon further heating the cementite plates begin to spheroidize. Next, needle-like  $\text{Mo}_2\text{C}$  particles nucleate and grow as discussed previously.

$\text{Cr}_7\text{C}_3$  forms by nucleation either within the cementite particles or at the ferrite/cementite interface.  $\text{M}_{23}\text{C}_6$  is believed(37) to nucleate at cementite boundaries where  $\text{Cr}_7\text{C}_3$  is not already present.  $\text{M}_{23}\text{C}_6$  grows at the expense of both cementite and  $\text{Mo}_2\text{C}$ , thus reducing the total number of particles.

Baker and Nutting implied that all carbides eventually form  $\text{M}_6\text{C}$  (see previous diagram). Lietnaker,

et al(40) found that this equilibrium carbide (called eta carbide) has a M/C ratio of approximately 4 rather than 6. The exact carbon content of this precipitate can be influenced by the chromium or oxygen content. Eta carbide may form at the expense of  $Mo_2C$ ,  $M_{23}C_6$ , or  $Cr_7C_3$ . It is believed to be nucleated at the interfaces between existing carbides and the matrix.

3. Welding Metallurgy: In view of the complex carbide precipitation discussed previously, problems in the welding of 2 1/4 Cr - 1 Mo steel are anticipated, particularly with high heat input welding processes. As a result of the varied thermal history from the fusion zone to the unaffected base metal, a large variation in mechanical properties and microstructure can be expected. To eliminate these problems a post-weld heat treatment is usually employed. This heat treatment must be at a high enough temperature (~1200F) to avoid post-weld stress relief embrittlement. The heat treatment tends to equalize the differences in microstructure and mechanical properties.

4. Carbide Stability in Lithium: An important factor in the lithium corrosion of 2 1/4 Cr - 1 Mo steel is the relative thermodynamic stability of each of the carbides. The free energies of formation of several of the carbides formed in this steel along with the free energy of formation

of lithium carbide are plotted in Figure 3.

According to Figure 3 cementite and  $\text{Mo}_2\text{C}$  are unstable in lithium below  $\sim 700\text{C}$ . These carbides should decompose in the presence of lithium to form  $\text{Li}_2\text{C}_2$ . The reaction involving the decomposition of cementite by lithium has been directly observed by Beskorovainyi, et al(14,32).

#### Experimental Scope

Preliminary screening tests performed at the Colorado School of Mines(1) indicate that corrosion rates of parent metal 2 1/4 Cr - 1 Mo in high-nitrogen liquid lithium are less than those found for 304 stainless steel. However, significant grain boundary penetration in heat-affected zones of Gas Tungsten Arc (GTA) welded coupons of 2 1/4 Cr - 1 Mo was also observed. This investigation was devoted to a systematic study of this phenomena. GTA-welded coupons of both regular grade and Nb-stabilized 2 1/4 Cr - 1 Mo steel were given various post-weld heat treatments and subsequently exposed to low-nitrogen lithium at 500C. The lithium bath contained 17.6 weight percent lead because current "heavy ion driver" fusion reactor designs utilize a lithium-lead liquid of this composition for the protective blanket. Additional corrosion tests were performed with coupons deliberately made corrosion susceptible. These

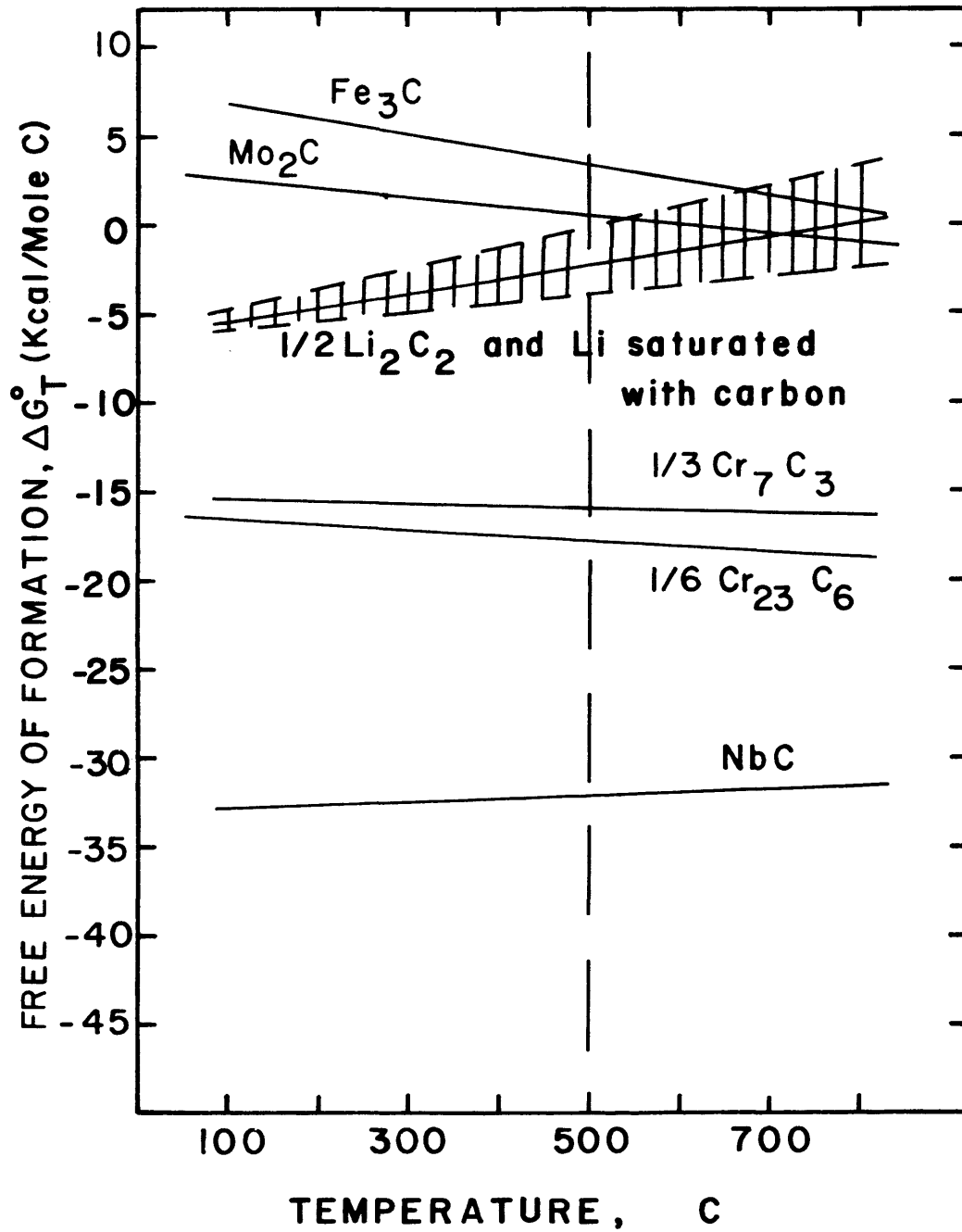


Figure 3. Relative thermodynamic stability of several carbides in carbon saturated lithium(14).

coupons were tested in lithium-lead at various temperatures for the purpose of measuring activation energies which provide insights into corrosion mechanisms.

It was not the purpose of this investigation to examine the effect of lead content on the corrosiveness of liquid lithium. Since parallel corrosion tests with pure lithium were not performed, it was not possible to compare the corrosion of 2 1/4 Cr - 1 Mo by lithium lead with the corrosion of the steel by lithium. All corrosion models and proposed mechanisms discussed in this thesis do not consider the role of lead.

EXPERIMENTAL PROCEDURE

The chemical compositions of the two alloys used in this investigation are shown in Table I.

TABLE I

Chemical Compositions of the 2 1/4 Cr - 1 Mo Alloys (wt%)

<u>Alloy</u>	<u>C</u>	<u>Si</u>	<u>Mn</u>	<u>P</u>	<u>S</u>	<u>Cr</u>	<u>Ni</u>	<u>Mo</u>	<u>Nb</u>	<u>Fe</u>
Regular Grade 2-1/4Cr-1Mo	0.12	0.32	0.43	0.018	0.002	2.07	--	1.04	--	bal.
Nb-Stabilized 2-1/4Cr-1Mo	0.09	0.32	0.46	0.012	0.007	2.19	0.55	0.98	1.13	bal.

Corrosion of GTA Weldments

The metallurgical conditions of weldments (see Fig. 4) of both the unstablized and niobium-stablilized compositions shown in Table I were varied by post-weld heat treatments representing the minimum and maximum temperatures specified by code. The geometry of the weldment coupons is shown in Figure 4. The data matrix for this investigation is shown in Table II. Isothermally transformed and tempered coupons of both Nb-stabilized and regular grade 2 1/4 Cr - 1 Mo

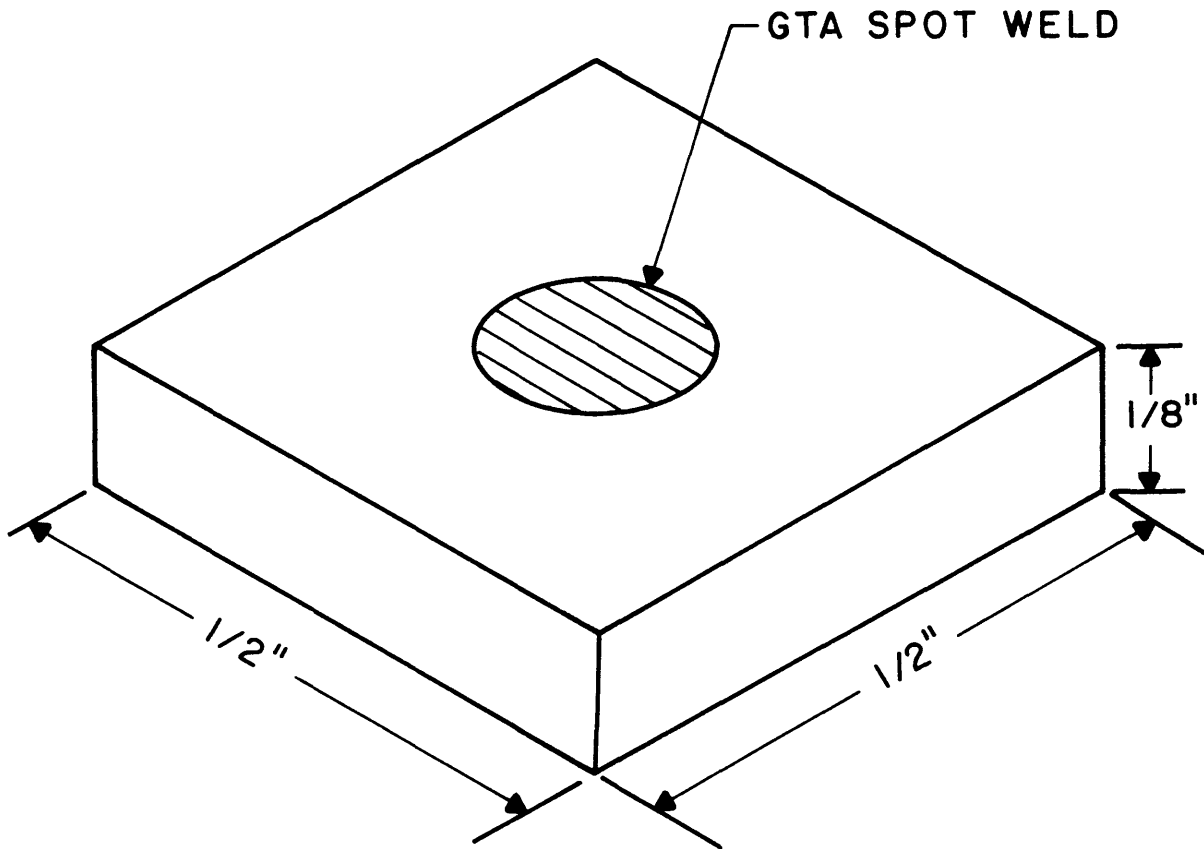


Figure 4: Schematic of a GTA-welded coupon. Unwelded coupons of similar geometry were used for the weight loss and simulated weldment studies.

TABLE II

## LIQUID LITHIUM CORROSION

## OF 2¼ CR - 1 Mo STEEL WELDMENTS

A. 17.6 w/o Pb IN LITHIUM

B. HEAT TREATMENT: AUSTENITIZED (927C) COOLED @ 50 c/HR TO 704C, ISOTHERMALLY TRANSFORMED @ 704C (2 HRS), COOLED @ 50 c/HR TO 500C, FURNACE COOLED, TEMPERED @ 760C FOR 10 HRS.

C. PRE-HEAT: 200C

ALLOY	POST WELD HEAT TREATMENT		
	NONE	10 HRS @ 710C	10 HRS @ 760C
2¼ CR - 1 Mo NB-STABILIZED	*	*	*
2¼ CR - 1 Mo UNSTABILIZED	*	*	*

EXPOSURE TIME: 1600 HRS

steel were preheated, Gas Tungsten Arc (GTA) welded, then given one of the post-weld heat treatments listed in Table II.

The GTA-welded coupons, along with unwelded coupons for weight loss measurements, were suspended by iron wires in a 2 1/4 Cr - 1 Mo crucible containing molten lithium (with 17.6 w/o lead) at 500 C. The maximum exposure time was 1600 hrs. Figure 5 shows a diagram depicting the apparatus used. The crucible was heated by means of an electric resistance furnace, controlled to  $\pm 2$ C by a thermocouple placed in a well in the crucible. Prior to each test a thermocouple was briefly immersed in the lithium to determine the actual lithium temperature. Coupons were removed from the lithium at various times and were examined metallographically. All coupons were mounted, polished, and etched in 2% nital for 25-30 seconds. A microscope equipped with a measuring eyepiece was used to measure the depth of lithium penetration.

2 1/4 Cr - 1 Mo steel crucibles were used to prevent dissimilar metal effects. After each test, the furnace was cooled down to room temperature and the crucible was removed for cleaning. The crucible contained approximately 100g of solid lithium-lead. The spent lithium was dissolved by immersing the crucible in a large container of tap water

T-2372

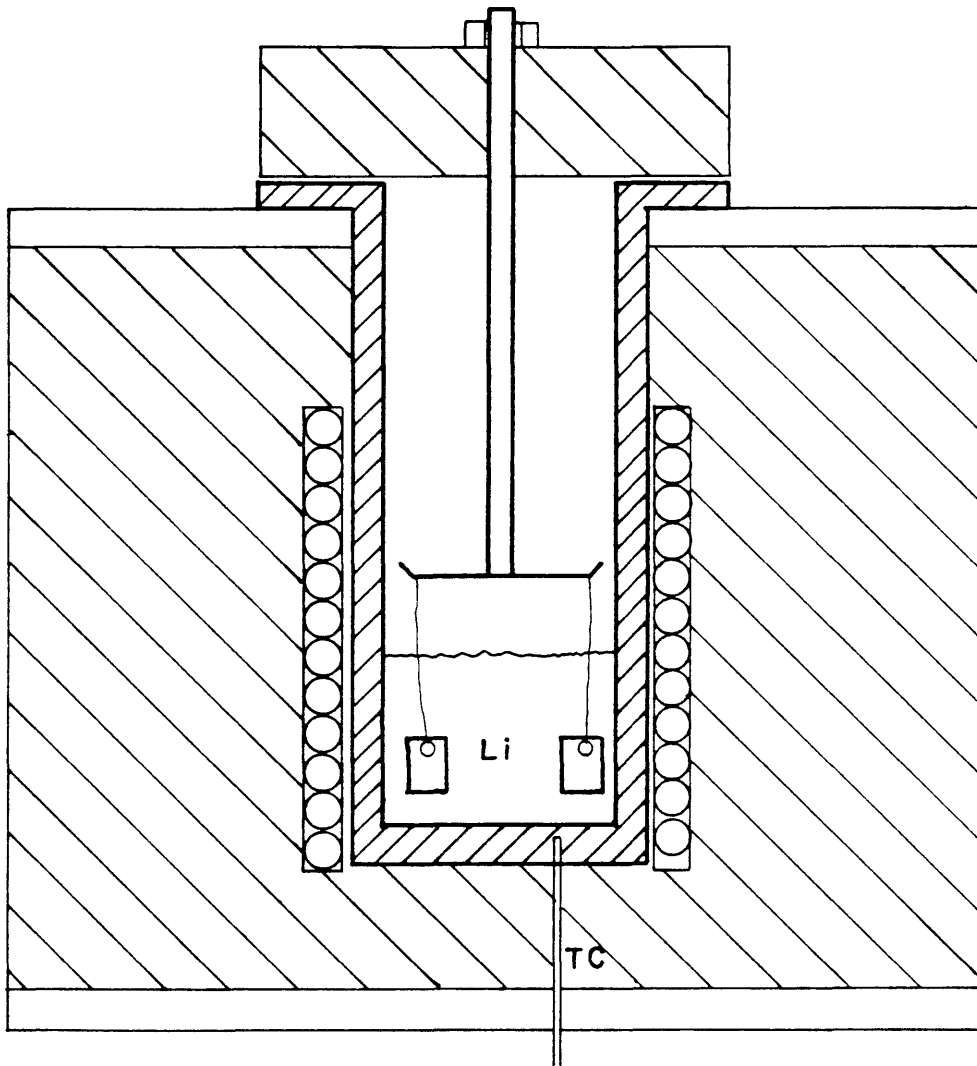


Figure 5: Schematic drawing of apparatus used in weight loss and penetration studies.

which was placed under a fume hood. When all of the lithium had dissolved, the crucible was rinsed thoroughly. Prior to the next test the inside of the crucible was sand blasted to remove any corrosion product and to expose a clean steel surface.

All tests were performed in an inert atmosphere glove box. Atmosphere purification equipment maintained the atmosphere at approximately 100 ppm O<sub>2</sub> and 400 ppm N<sub>2</sub>. This relatively pure atmosphere made it possible to maintain the nitrogen content in the lithium at a very low value (<100 ppm) when the crucible lid was kept in place. During a test, samples of lithium were periodically removed for nitrogen analysis by means of the micro-Kjeldahl technique(22). The lithium sampling technique used in this investigation is illustrated in Figure 6. The sampling apparatus is comprised of a 304 stainless steel tube connected to two valves. With the chamber between the valves evacuated, the sampling tube is immersed in the lithium. The lower valve is opened, drawing lithium into the tube. The sampler is removed from the lithium and allowed to cool. With the sample still in a protective atmosphere, a section is cut out of the tube and placed in an air-tight container. The container is then brought outside of the glove box where the sample is immediately

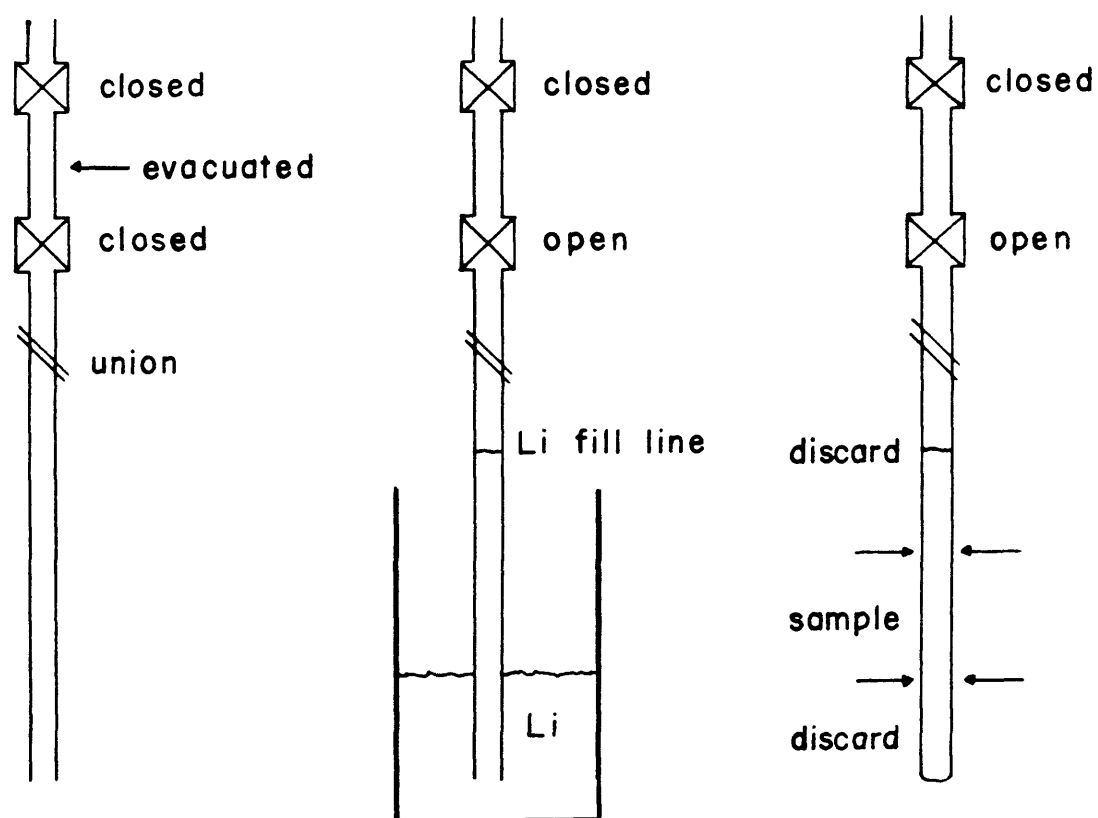


Figure 6: Schematic of the lithium sampling technique.

analyzed. Typical measurements of nitrogen content ranged from 45 to 65 ppm, nitrogen levels which approach the limit of detectability for the technique.

#### Corrosion of Simulated Weldments

To more fully understand the intergranular penetration seen in weld heat affected zones, corrosion tests were also performed on coupons which had been deliberately heat treated to give microstructures susceptible to lithium attack. Coupons of 2 1/4 Cr - 1 Mo were heat treated so as to produce the coarse-grained bainitic microstructures found in GTA-weld heat affected zones(41). This was accomplished by quenching specimens from three different austenitizing temperatures (1300C, 1150C, 927C) at three different cooling rates (water quench, oil quench, air cool). After heat treatment the scale was removed from the surface of the steel by grinding. All coupons were ground to 600 grit.

These coupons were exposed to lithium-17.6 w/o lead at temperatures ranging from 400C to 625C. The coupons were sectioned after exposure and examined metallographically. All coupons were etched in 2% nital for 25-30 seconds. Penetration was measured at various places on a given coupon; the simple mean was calculated and plotted on a penetration vs. time<sup>1/2</sup> curve. The corresponding corrosion rates were plotted on an Arrhenius plot to determine

activation energies.

### Stress Tests

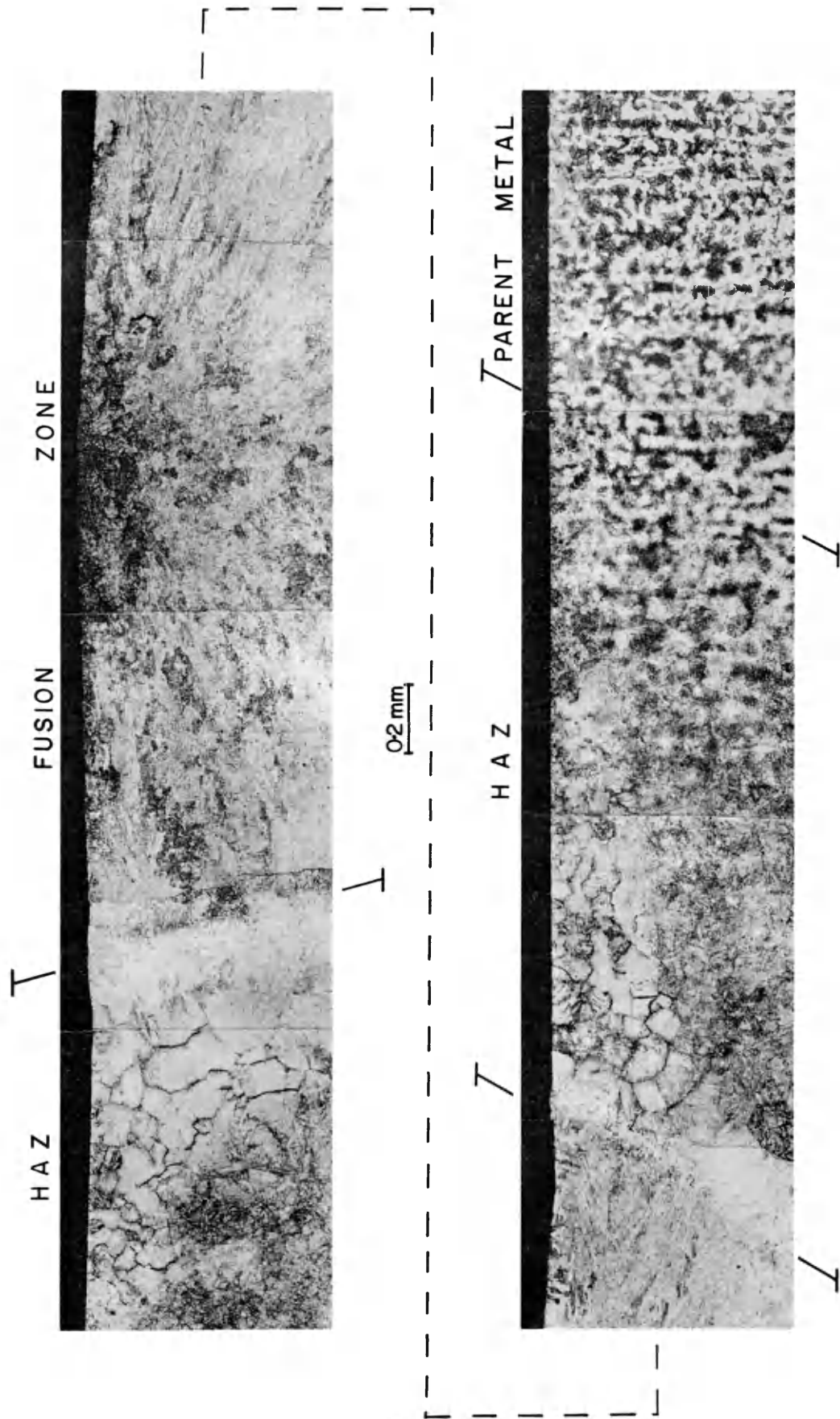
An attempt was made to determine the effect of stress on the lithium penetration rate of the weld heat-affected zone of 2 1/4 Cr - 1 Mo steel. A tensile specimen with a GTA-weld was placed in lithium-17.6 w/o lead at 500C for 400 hrs. A stress of 18 ksi was applied by a constant load creep apparatus. Next, tensile specimens, each with variable cross-sectional area, were given a weld-simulating heat treatment and were subsequently stressed in the lithium-lead liquid at 500C. Nominal applied stresses ranged from 20 to 40 ksi in each specimen.

## RESULTS AND DISCUSSION

### Corrosion of GTA Weldments

Figures 7&8 are micrographs of two regular grade weldments, one with no post-weld heat treatment and the other with a post-weld heat treatment of 10 hrs. at 760C. These figures illustrate the effect of post-weld heat treatment on the microstructure and the relative amount of lithium attack after ~700 hours of exposure. Note the severe intergranular attack at prior austenitic grain boundaries in the heat-affected zone of the weldment with no post-weld heat treatment (Figure 7). The Nb-stabilized weldment (shown in Figure 9) along with the regular grade weldment in Figure 8 (10 hrs @ 760C post-weld H.T.) seem to be highly resistant to lithium attack. Figure 10 shows a higher magnification comparison of the tempered vs. untempered heat-affected zone microstructures. These micrographs further illustrate the dramatic improvement in lithium corrosion resistance afforded the weldments of regular grade 2 1/4 Cr - 1 Mo steel by a high temperature post-weld heat treatment. The post-weld heat treatment has a dramatic effect on the appearance of the HAZ microstructure (Figure 10). Many of the carbides in Figure 10b have spheroidized and prior austenitic grain boundaries

2 1/4Cr-1Mo STEEL EXPOSED AT 500 C TO LIQUID LITHIUM CONTAINING 17.6% LEAD

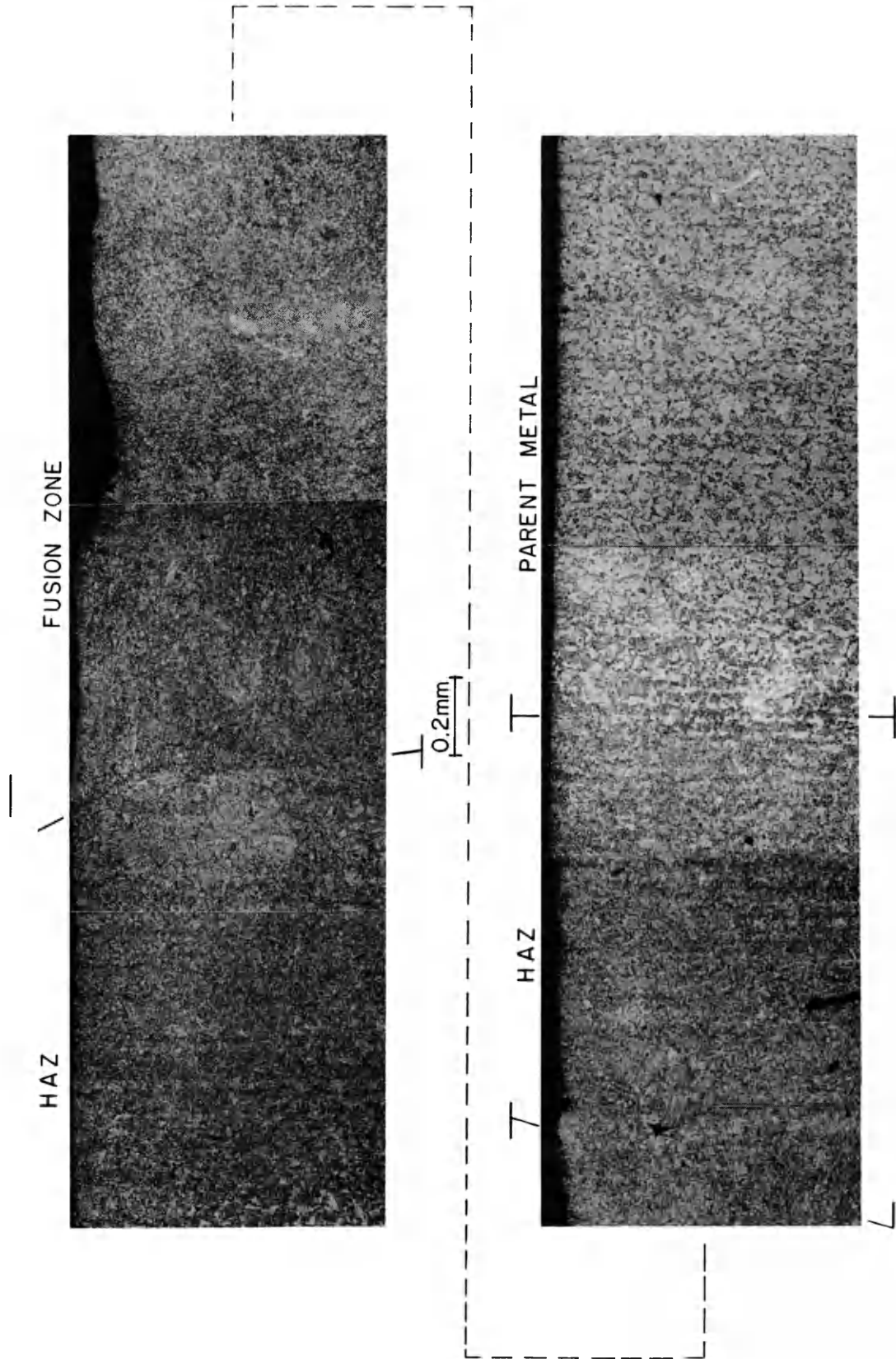


NO POST WELD HEAT TREATMENT

EXPOSURE TIME: 711 hrs

Figure 7: Intergranular penetration of a 2 1/4 Cr-1 Mo (regular grade) GTA weldment at prior austenitic grain boundaries in the heat affected zone.

2 1/4 Cr-1 Mo STEEL EXPOSED AT 500C TO LIQUID LITHIUM CONTAINING 17.6% LEAD



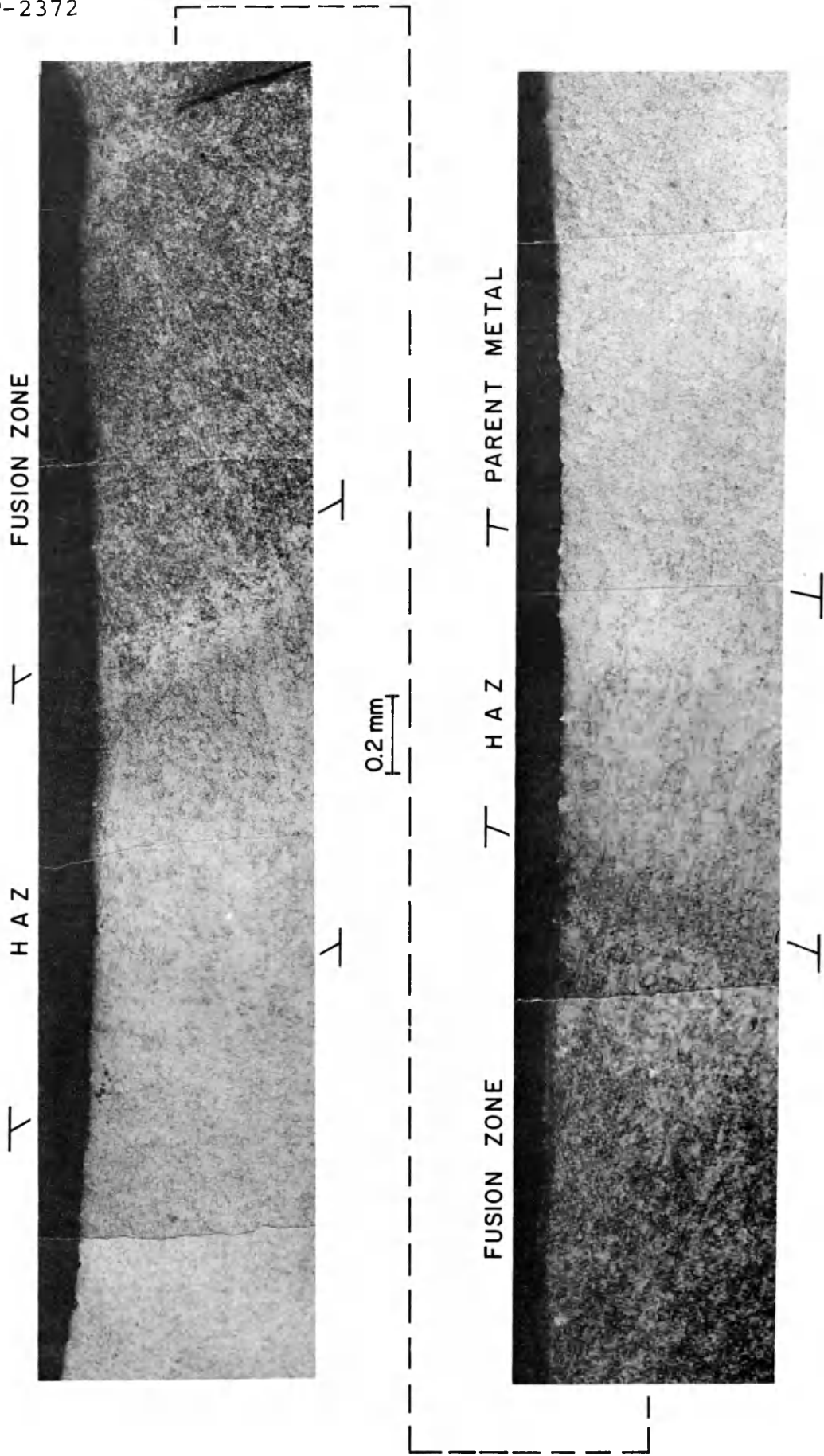
POST WELD HEAT TREATMENT : 10 hrs at 760C

EXPOSURE TIME: 711 hrs

Figure 8: A regular grade 2 1/4 Cr-1 Mo GTA weldment (10 hrs. @ 760C post-weld heat treatment) exposed to lithium-17.6 w/o lead at 500C.

Nb-STABILIZED 2 1/4 Cr-1 Mo STEEL EXPOSED AT 500 C TO LIQUID LITHIUM CONTAINING 17.6% LEAD

T-2372



NO POST WELD HEAT TREATMENT

EXPOSURE TIME : 758 hrs

Figure 9: Nb-stabilized 2 1/4 Cr-1 Mo GTA weldment (no post-weld heat treatment) exposed to Li-17.6 w/o Pb at 500C.

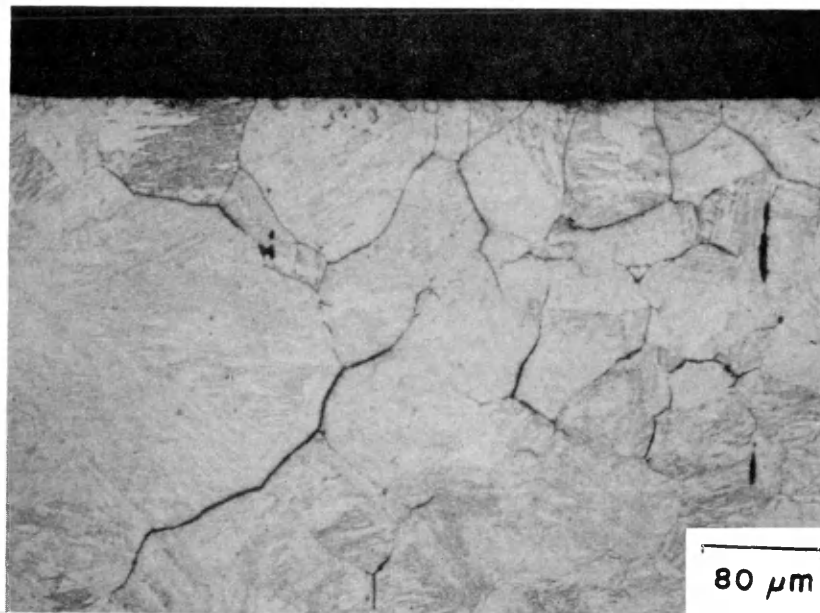


Figure 10a: Corrosion of a 2 1/4Cr-1Mo weld HAZ.  
No post-weld H.T.  
Exposure: 178 hrs in Li-17.6%Pb at  
500C.

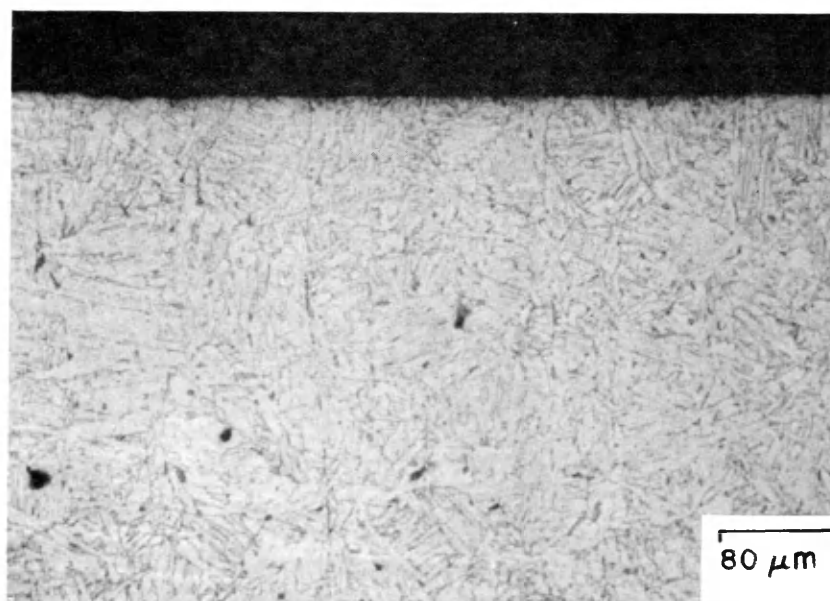


Figure 10b: Corrosion of 2 1/4Cr-1Mo weld HAZ.  
Post-weld H.T.: 10 hrs @ 760C.  
Exposure: 178 hrs in Li-17.6%Pb  
at 500C.

are barely visible in Figure 10b.

The susceptibility of the various metallurgical conditions to lithium corrosion is summarized on a penetration vs time<sup>1/2</sup> curve in Figure 11. Time<sup>1/2</sup> was chosen for the x-axis because previous data follows parabolic rate kinetics(1,6,7,13,14,22-24). The regular grade material with no post-weld heat treatment experienced the most rapid corrosion, especially during initial stages of attack. This curve exhibits a change in slope which will be discussed later. A GTA weldment was subjected of an 18 ksi stress during exposure to Li-17.6% Pb. This test yielded a single data point which lies fairly close to the penetration vs. time<sup>1/2</sup> curve for unstressed weldments (Figure 11).

The weldment of the niobium-stabilized 2 1/4 Cr - 1 Mo steel (Figure 9) has a much more homogeneous microstructure than the regular grade weldment in Figure 7. Nb-stabilized weldments were quite resistant to corrosion by low nitrogen (~50 ppm) lithium-17.6 weight percent lead. Only slight penetration (near the limit of measurement) was observed after 1400 hours, and the heat-affected zones of the welds were not preferentially attacked. Figure 12 shows the penetration of the Nb-stabilized parent metal. The depth and morphology of the attack is similar in the heat-affected

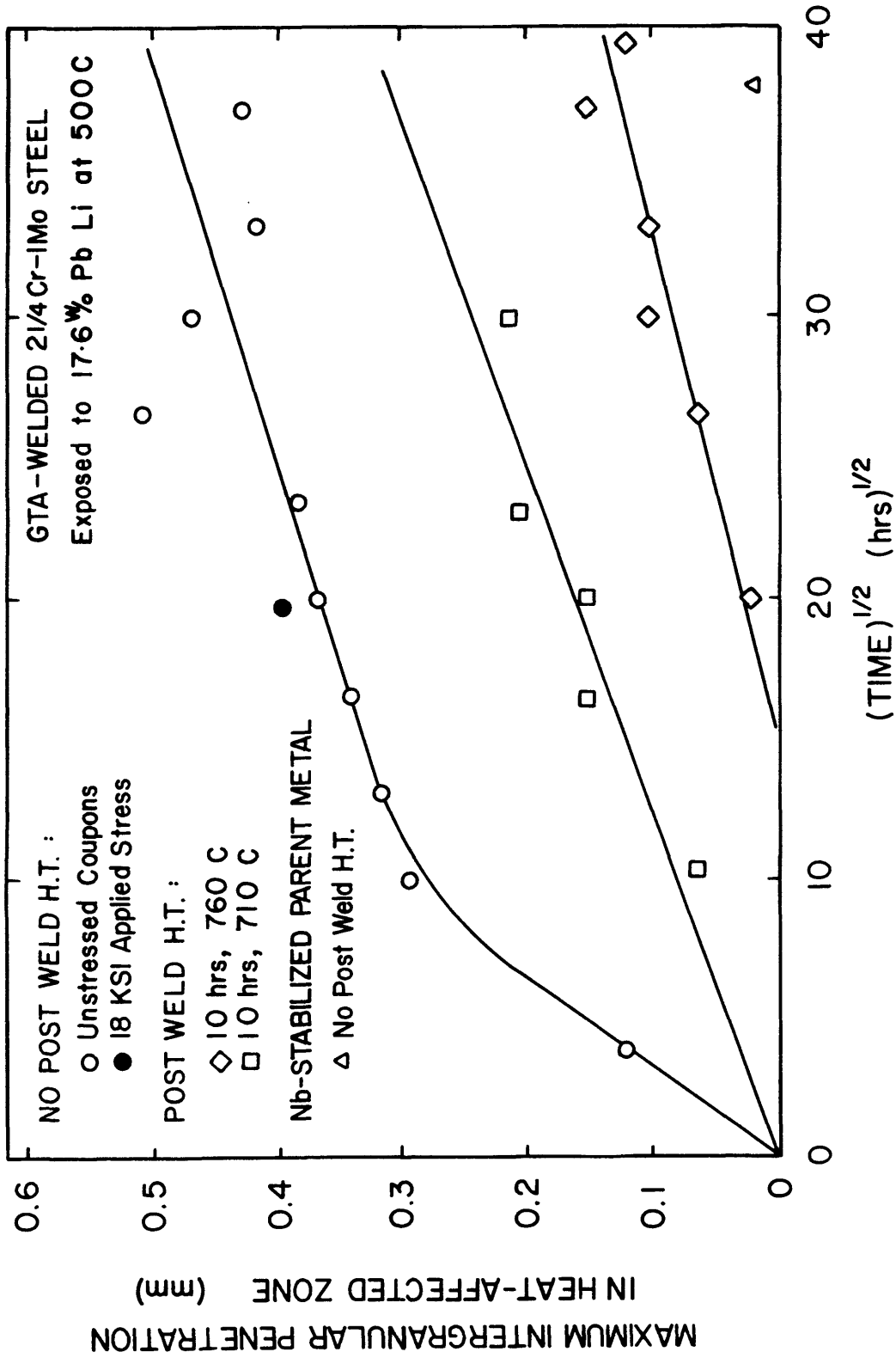


Figure 11: Penetration vs time<sup>1/2</sup> as a function of post-weld heat treatment and niobium content of GTA weldments exposed to Li-17.6 w/o Pb at 500C.

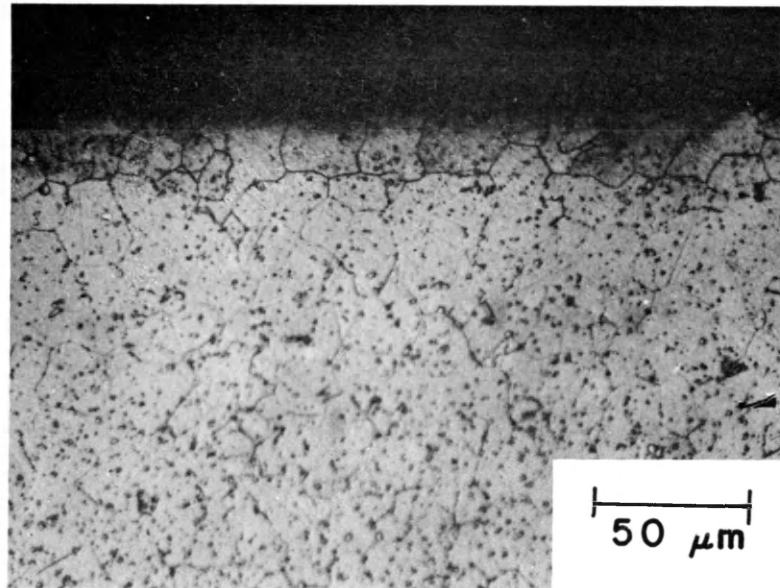


Figure 12: Corrosion of the Nb-stabilized  
2 1/4 Cr-1 Mo parent metal.  
No post-weld H.T.  
Exposure: 1464 hrs in  
Li-17.6%Pb at 500C.

zone. Post-weld heat treatments did not significantly affect the corrosion resistance of Nb-stabilized 2 1/4 Cr - 1 Mo steel in lithium-lead.

Post-weld heat treatments of regular grade 2 1/4 Cr - 1 Mo weldments change the morphology of the lithium attack as well as dramatically improve the corrosion resistance. Optical and SEM micrographs in Figures 13&14 show the highly localized "worm hole" penetration in the heat-affected zones of post-weld heat treated specimens (regular grade) exposed to lithium for times up to 1344 hours. The lithium appears to attack acicular second phase particles in the matrix rather than prior austenitic grain boundaries(Figure 14).

The corrosion resistance of a given microstructure of 2 1/4 Cr - 1 Mo steel in lithium-lead can be related to the carbide composition and morphology of the material. Figure 3 indicates that while cementite and  $\text{Mo}_2\text{C}$  are unstable in lithium at 500C, carbides formed during later stages of tempering (such as  $\text{M}_{23}\text{C}_6$ ) are stable and therefore are not susceptible to lithium attack. Since the heat-affected zone of a GTA weldment is subjected to an austenitizing treatment and a post-weld heat treatment is merely a tempering treatment, the Baker and Nutting(37) study of quenched and tempered 2 1/4 Cr - 1 Mo steel can be utilized to determine carbides present in the various metallurgical conditions of

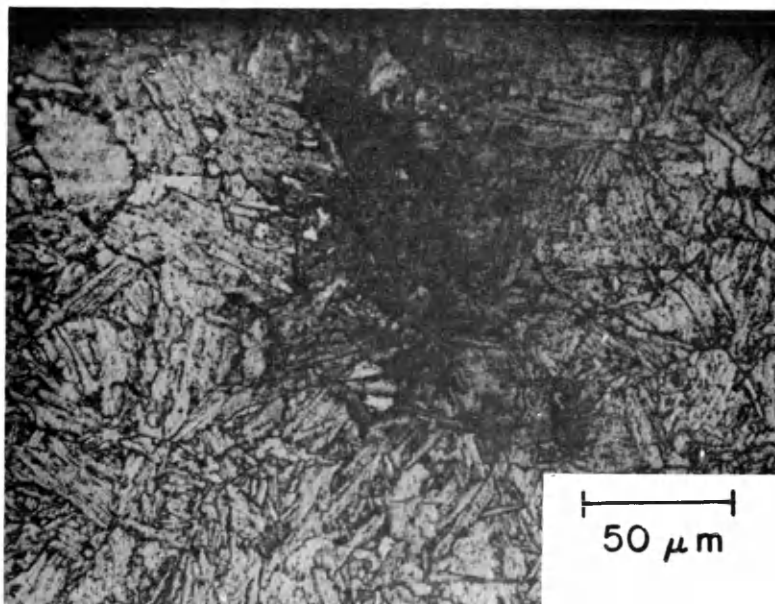


Figure 13a: Corrosion of a 2 1/4 Cr - 1 Mo weld HAZ.  
Post-weld H.T: 10 hrs @ 710C.  
Exposure: 300 hrs in Li-17.6%Pb at 500C.

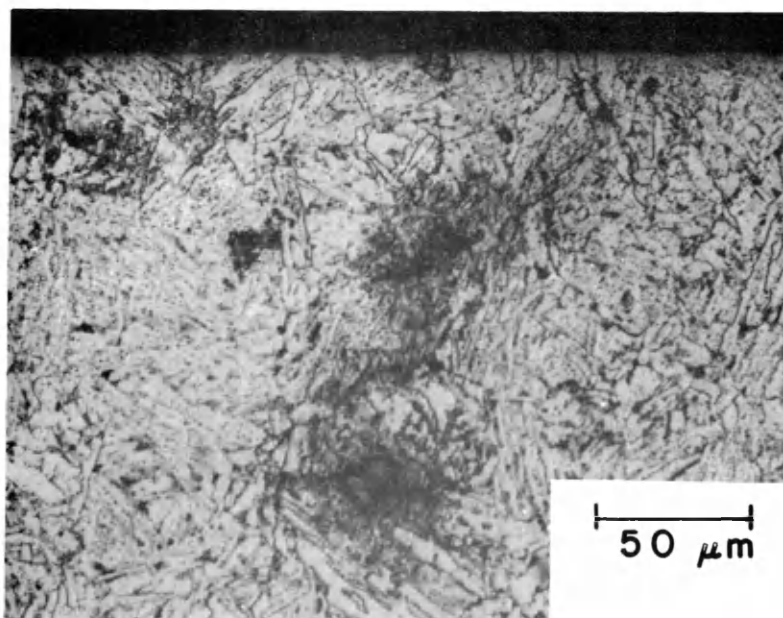
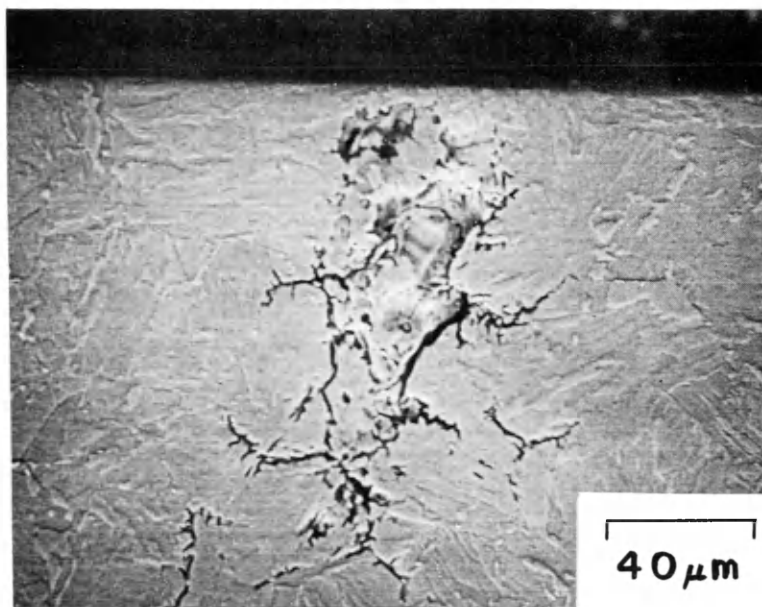
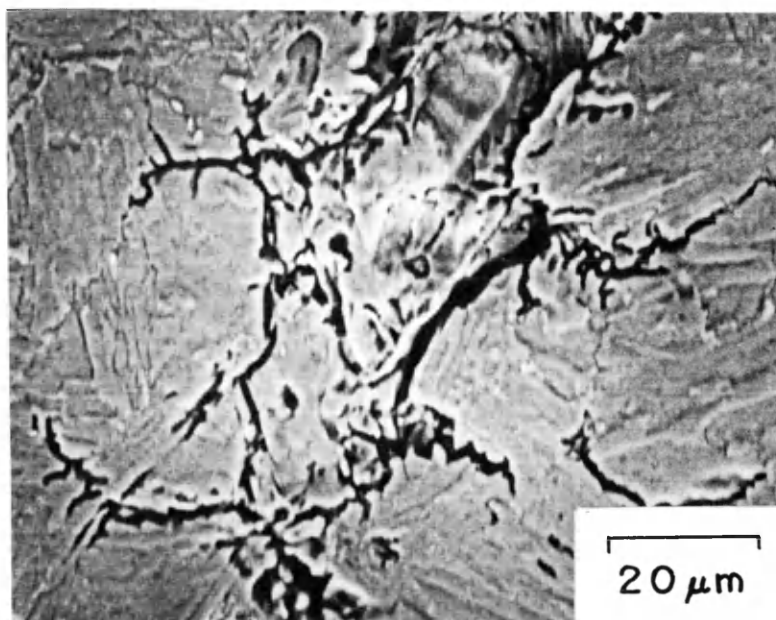


Figure 13b: Corrosion of a 2 1/4 Cr - 1 Mo weld HAZ.  
Post-weld H.T: 10 hrs @ 760C.  
Exposure: 1344 hrs in Li-17.6%Pb at 500C.



(a)



(b)

Figure 14: SEM micrographs of HAZ corrosion.  
Post-weld H.T: 10 hrs @ 710C.  
Exposure: 300 hrs in Li-17.6% Pb at 500C.  
(b) is higher magnification of the image in (a).

the weldments. The Baker and Nutting carbide stability diagram for the quenched steel is shown in Figure 15. When 2 1/4 Cr - 1 Mo steel is cooled rapidly from an austenitizing temperature a mixture of cementite and  $\epsilon$ -carbide precipitates in a bainitic and/or martensitic matrix. It is believed believe that intergranular penetration of the regular grade weldments is a result of the dissolution of cementite and/or  $\epsilon$ -carbide by the lithium. The  $\epsilon$ -carbide is less stable than cementite. Since cementite is thermodynamically unstable in lithium (Figure 3)  $\epsilon$ -carbide must also be unstable in lithium. The mechanisms underlying the corrosion of this microstructure are discussed in greater detail in the section of this thesis which describes the corrosion of simulated weldments.

As was noted previously, the corrosion of coupons with post-weld heat treatments has a different appearance. The attack does not follow prior austenitic grain boundaries as was the case in the untempered heat-affected zones.

According to Figure 15 the post-weld heat treatments should remove nearly all of the  $\text{Fe}_3\text{C}$  from the microstructure. The microstructure should contain primarily stable carbides such as  $\text{Cr}_7\text{C}_3$  and  $\text{M}_{23}\text{C}_6$ . However Figure 2 shows that  $\text{Mo}_2\text{C}$  will be present after tempering for 10 hrs. at 760C or 710C. A portion of a weld HAZ will approximate a

T-2372

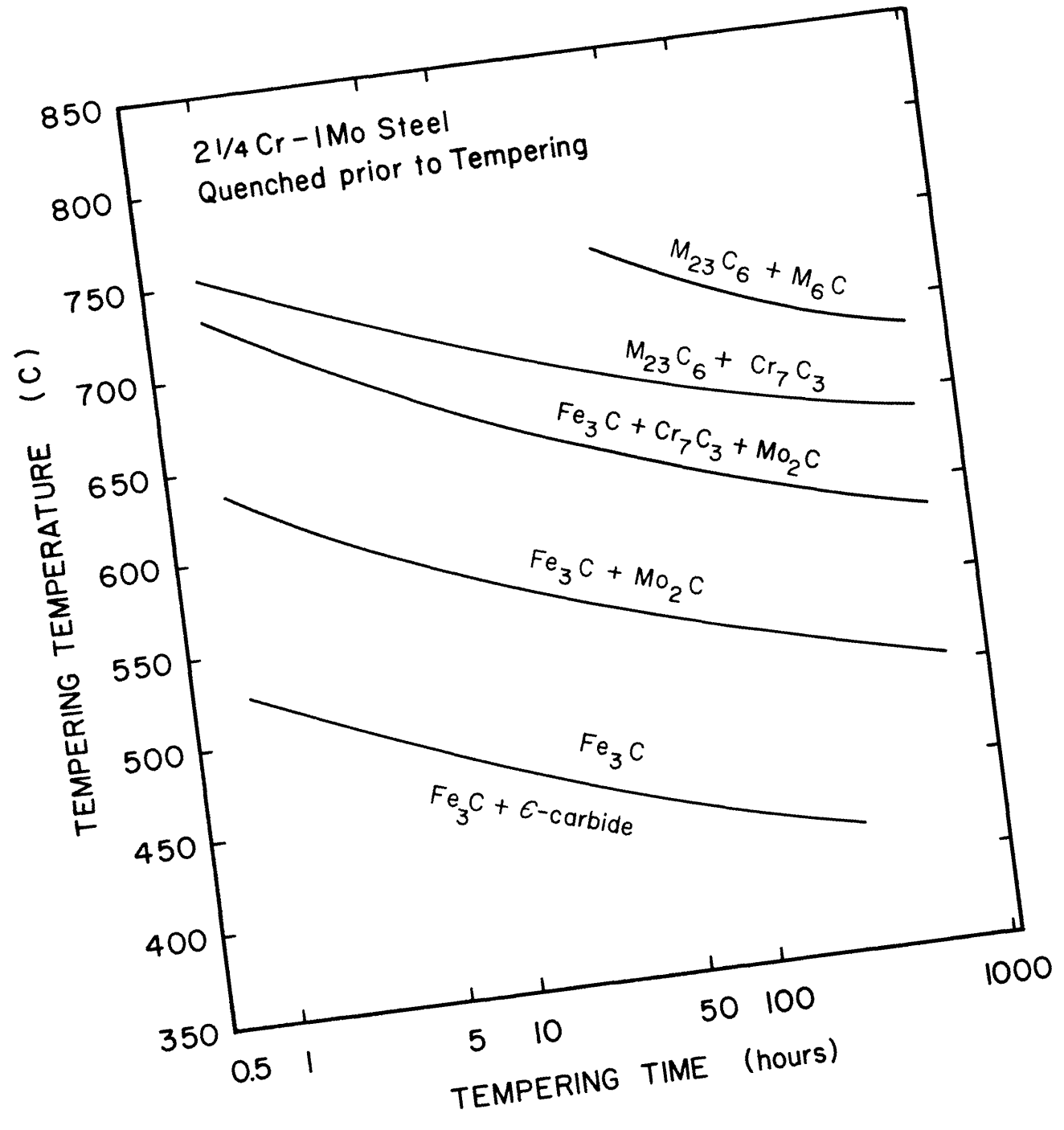


Figure 15: Carbides formed during the tempering of quenched 2 1/4 Cr - 1 Mo steel (37).

normalized microstructure. After post-weld tempers, "normalized" areas of the HAZ will contain  $\text{Mo}_2\text{C}$  which, according to Figure 3, is unstable in lithium.

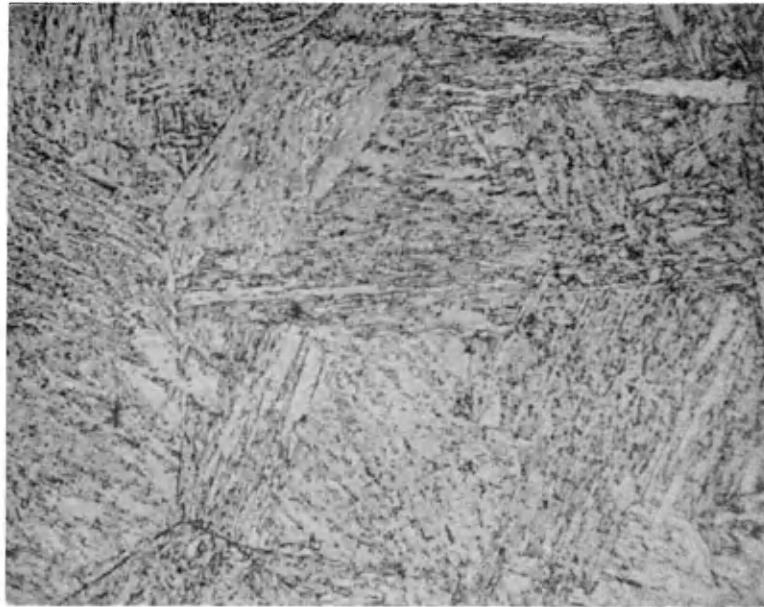
During tempering needle-like  $\text{Mo}_2\text{C}$  particles (referred to by Baker and Nutting as fringes) grow out from carbide-ferrite boundaries. The appearance of the attack in Figures 13&14 suggests that the lithium penetration follows a path set down by  $\text{Mo}_2\text{C}$  fringes. Further tempering at sufficiently high temperatures would remove the  $\text{Mo}_2\text{C}$  fringes and increase corrosion resistance. This is evidenced by the greater corrosion resistance of the 760C post-weld heat treatment (see Figure 11).

The niobium-stabilized alloy was extremely resistant to intergranular attack, even when no post-weld heat treatment was applied. This corrosion resistance can be attributed to the formation of stable refractory carbides upon cooling. Since these niobium carbides form rather than cementite, a post-weld heat treatment is not required for good corrosion resistance. The disadvantages of the niobium-stabilized alloy involve weldability, availability and the undesirable nuclear properties of two of the alloying elements, nickel and niobium.

### Corrosion of Simulated Weldments

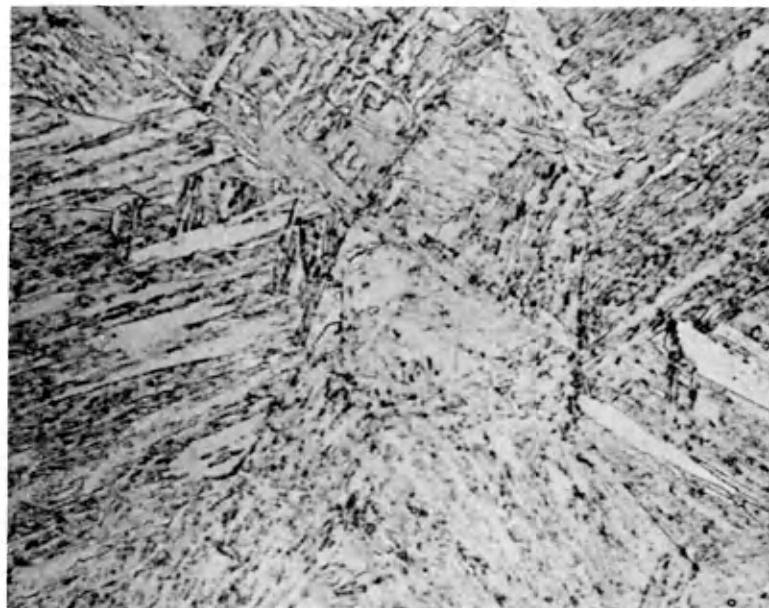
Coupons of regular grade 2 1/4 Cr - 1 Mo steel were heat treated so as to produce the coarse-grained bainitic microstructure found in the corrosion susceptible heat-affected zone of GTA weldments. The HAZ microstructure was best approximated by a 1300C austenitizing treatment followed by an oil quench. Figure 16 shows a comparison of the HAZ microstructure with the microstructure which was oil quenched from 1300C. These two microstructures have approximately the same prior austenitic grain size and the ferrite lath size and morphology are similar for both microstructures. These simulated weldments corroded intergranularly, as did the heat-affected zones of actual weldments. Figure 17 shows that significant intergranular attack occurred after only one hour of exposure to the 17.6% Pb-Li liquid at 500C.

The results of corrosion tests (at 500C) on specimens representing all the weld-simulating heat treatments are summarized in Figure 18. The penetration vs. time<sup>1/2</sup> curve for the GTA-welded coupons is superimposed for comparison. An obvious feature of Figure 18 is a change in slope in the penetration curves at approximately 25 hours. Note the increase in initial penetration rate caused by an increase in austenitizing temperature, and the insensitivity of the



HEAT-AFFECTED ZONE  
GTA-WELDED 2 1/4 Cr-1 Mo STEEL

25  $\mu\text{m}$



WELD-SIMULATING HEAT TREATMENT  
(AUSTENITIZED AT 1300 C, OIL-QUENCHED)

Figure 16: Comparison of microstructure from the heat affected zone of an actual GTA weldments and from a specimen heat treated (oil-quenched from 1300C) to simulate the weldment's heat affected zone.

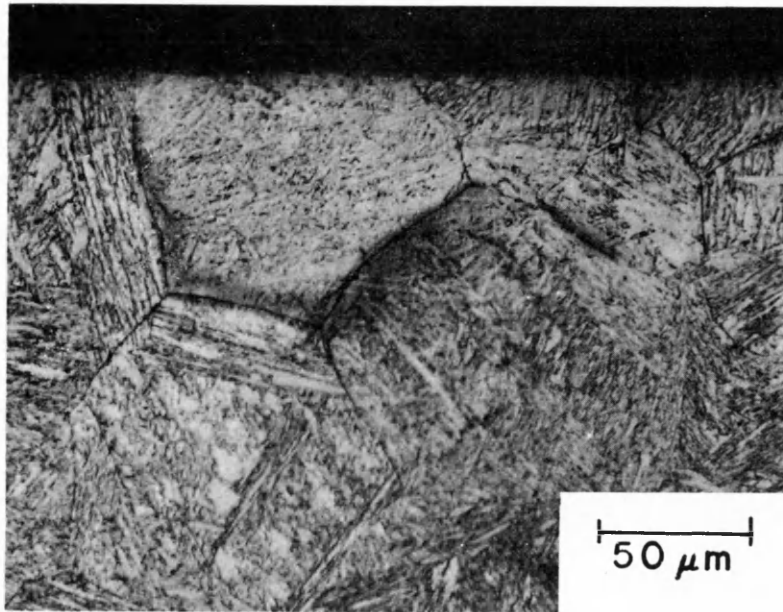


Figure 17: Intergranular penetration of a simulated HAZ (oil quenched from 1300C) specimen. Exposure: 1 hr in Li-17.6%Pb at 500C.

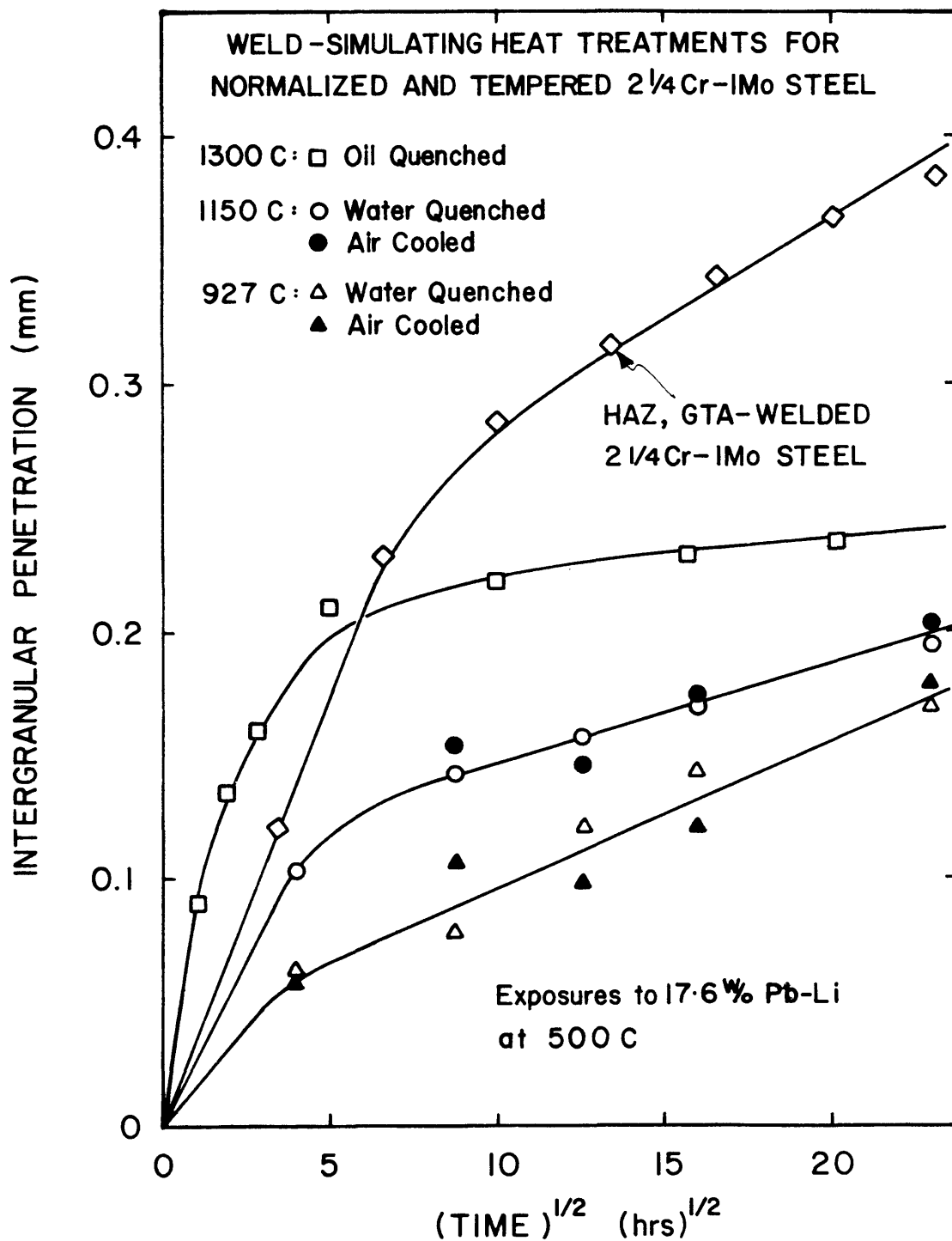


Figure 18: Intergranular penetration of 2 1/4 Cr - 1 Mo steel at 500C in lithium - 17.6 w/o lead as a function of time and heat treatment compared to the penetration of a GTA weldment of HAZ.

penetration rate to the cooling rate from the austenitic range. A possible explanation for the change slope in Figure 18 is associated with a phase transformation within the steel. When 2 1/4 Cr - 1 Mo is cooled rapidly from the austenitic range it transforms to a microstructure comprised of cementite and  $\epsilon$ -carbide precipitates in an acicular ferrite matrix. Upon tempering at 500C the less stable  $\epsilon$ -carbide is replaced by cementite (see Figure 15). According to Figure 15, the time required to replace  $\epsilon$ -carbide by tempering the steel at 500C is approximately the time at which the penetration curves in Figure 18 change slope. Since cementite is readily attacked by lithium at 500C and  $\epsilon$ -carbide is unstable relative to cementite in this steel, one would expect even more rapid lithium attack of any  $\epsilon$ -carbide present. A rapid penetration by lithium would result until  $\epsilon$ -carbide had been converted to cementite; then penetration would continue at a rate determined by the interaction of cementite with lithium.

The insensitivity of corrosion rate to cooling rate suggests the carbide composition and morphology in the bainite does not vary much with cooling rate. This observation is consistent with the data of Baker and Nutting(37) which show similar tempering characteristics for quenched and normalized steel. The possible reasons for the

dependence of corrosion rate on austenitizing temperature will be discussed later.

The results of Figure 18 alone are inconclusive; additional data are needed for a better understanding of corrosion mechanisms. A series of simulated weldment coupons (oil quenched from 1300C) were exposed to lithium-17.6% lead at temperatures ranging from 400-625C. The penetration vs. time<sup>1/2</sup> curves for the various temperatures are shown in Figure 19. The 500C penetration curve from Figure 18 (oil quenched from 1300C) is not included in Figure 19 (or Figure 21) because the coupons from the curve in Figure 18 were not heat treated the same way as the coupons used to generate Figure 19. The initial 1300C austenitizing treatment (Figure 18 curve) was done in an induction furnace with an argon atmosphere where the time required to reach the 1300C temperature was approximately one minute. The subsequent 1300C treatment (Figure 19 curves) was done in air in a glow-bar furnace where the required austenitizing time was ~10 minutes. The difference in austenitizing time apparently has a drastic effect on the results (i.e. an increase in austenitizing time apparently results in an increase in corrosion rate) because the curve in Figure 18 does not correlate well with the data in Figure 19.

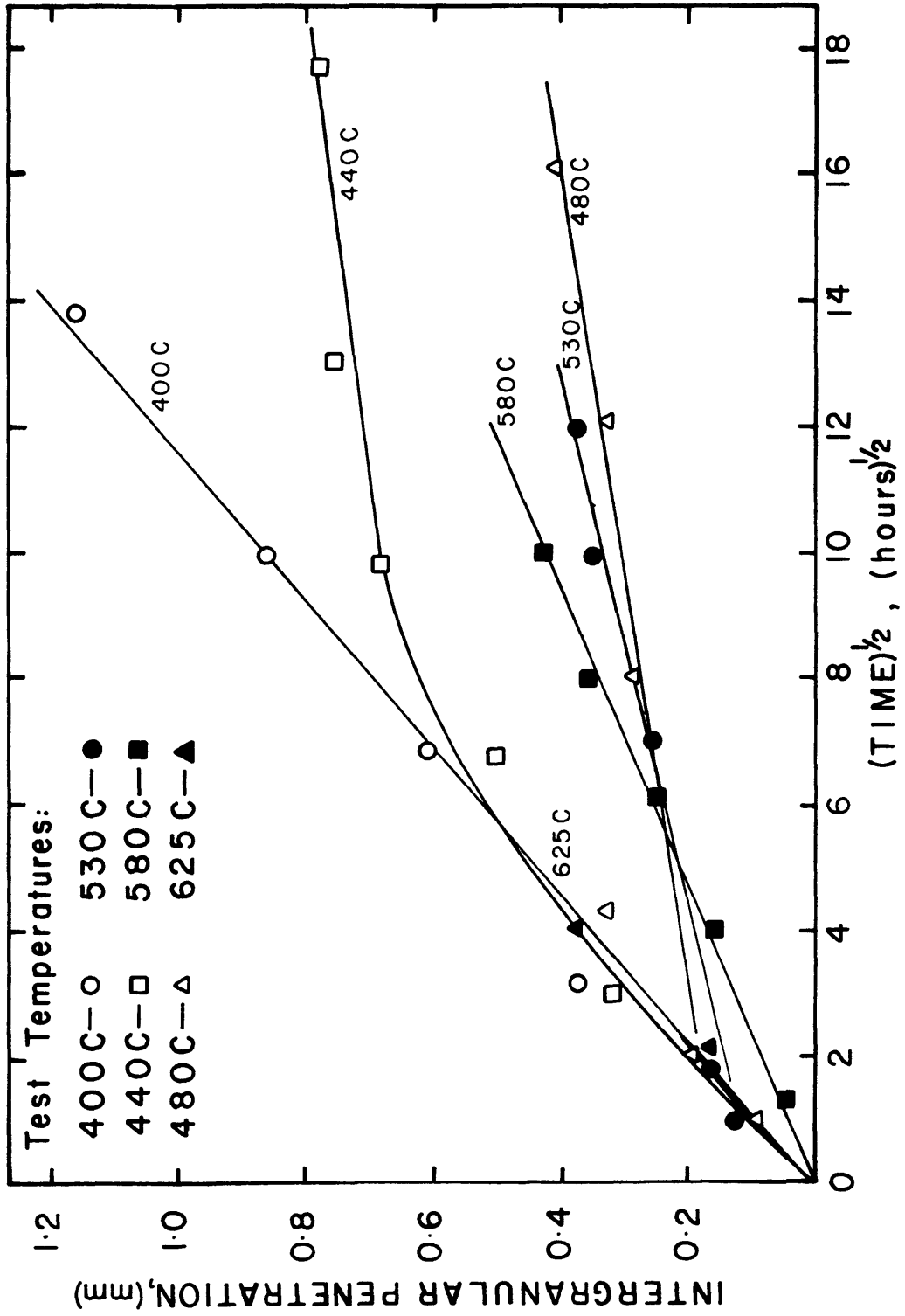


Figure 19: Corrosion of simulated weldments (oil quenched from 1300C) as a function of time<sup>1/2</sup> and temperature.

The corrosion tests performed at intermediate temperatures exhibit a change in slope, while both the higher and lower temperature corrosion data yield straight lines with no slope change. The time at which the slope changes increases with decreasing test temperature. Presumably, a change in corrosion rate would be observed at 400C if the duration of the test was greater. Slope changes at 580C and 625C may occur in time intervals too small to resolve.

The approximate slope change times as a function of temperature (from Figure 19) were plotted in Figure 20 along with the Baker and Nutting curve (from Figure 15) which depicts the transformation of  $\epsilon$ -carbide to cementite. The slope change times were estimated to be the intersection of the extrapolation of the straight-line portions of each curve. The fact that the two curves in Figure 20 have a similar shape lends credibility to the theory that the slope changes observed in Figures 18&19 are a direct result of the transformation of  $\epsilon$ -carbide to cementite. The difference in the relative positions of the two curves is probably caused by differences in alloy content. The steel used this investigation has slightly higher chromium and molybdenum contents than the alloy used by Baker and Nutting(37). Smith and Nutting(41) observed that chromium and molybdenum

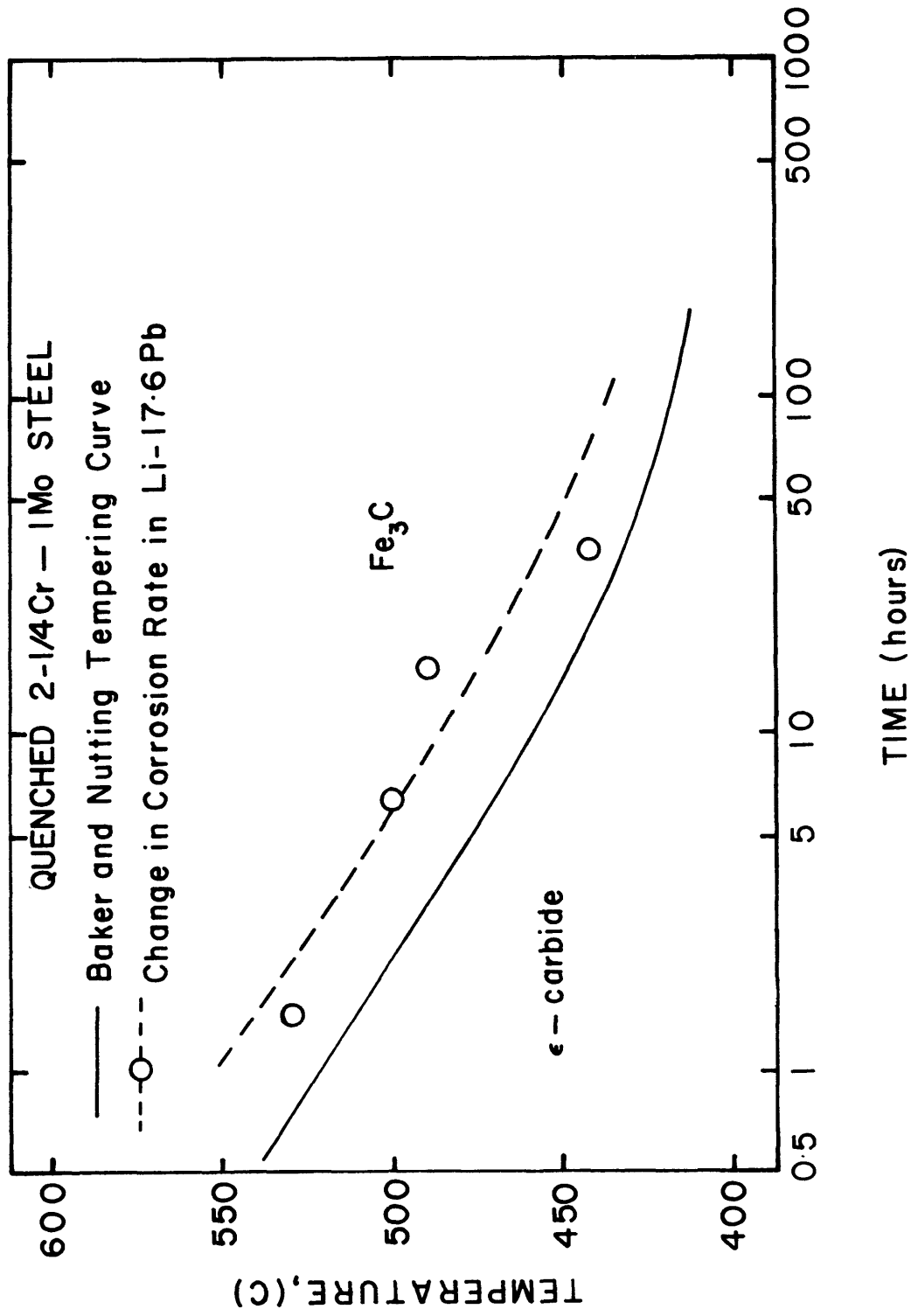


Figure 20: Comparison of the change in corrosion rate with the conversion of epsilon carbide to cementite in quenched 2 1/4 Cr - 1 Mo steel.

additions to steel tend to increase the metastability of  $\epsilon$ -carbide. Therefore, it is not surprising that the curve generated in this investigation lies to the right of the Baker and Nutting curve.

The slopes of the curves in Figure 19 were measured and the corresponding rate constants were plotted as a function of temperature on an Arrhenius plot (Figure 21). The Arrhenius expression suitably describes the temperature dependence of rate constants for intergranular penetration because the rate of "back-jump" over the activation barrier was estimated and was found to be negligible. The initial corrosion rate is controlled by a mechanism with an activation energy of 5.3 kcal/mole. The rate controlling step in the secondary corrosion process has an activation energy of 28 kcal/mole.

Corrosion models and proposed mechanisms based on experimental observations are described in the following pages. In all of the models discussed in this thesis, it is assumed that lead does not affect the corrosion mechanisms or the rate controlling steps. Apart from its effect on the activity of lithium, it is not known what role, if any, lead plays in the corrosion of this steel. Future work(43) is devoted an examination of the effect of lead content on the corrosion kinetics.

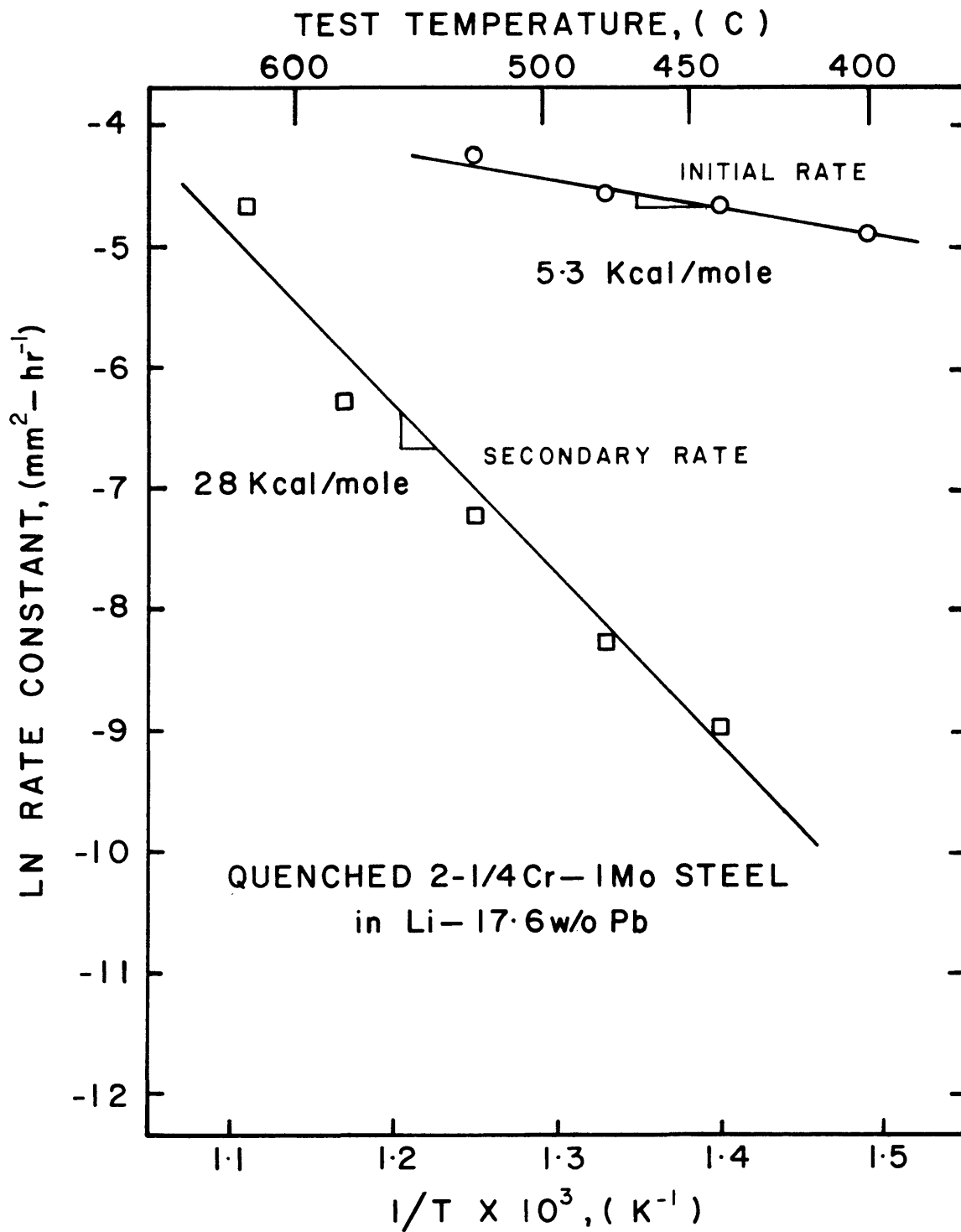
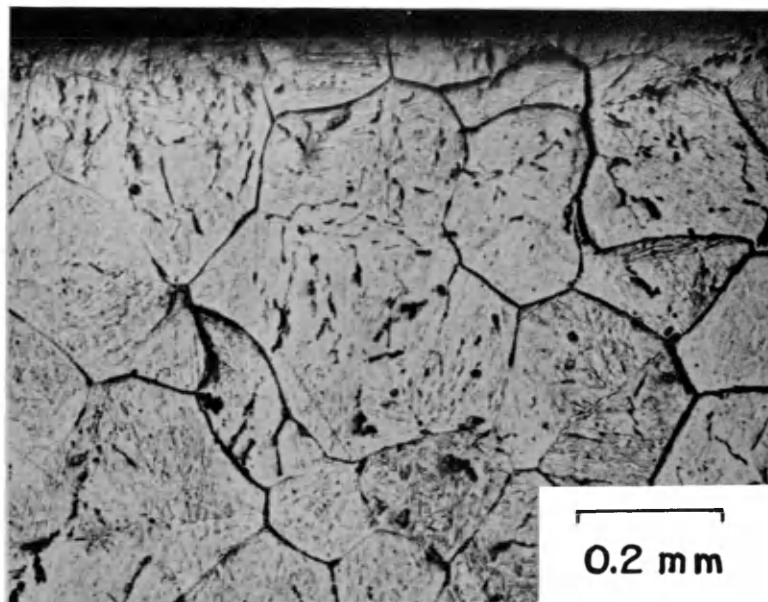


Figure 21: Arrhenius plot of the corrosion rate constant (penetration =  $(kt)^{1/2}$ ) as a function of temperature for simulated weldments (oil quenched from 1300C.).

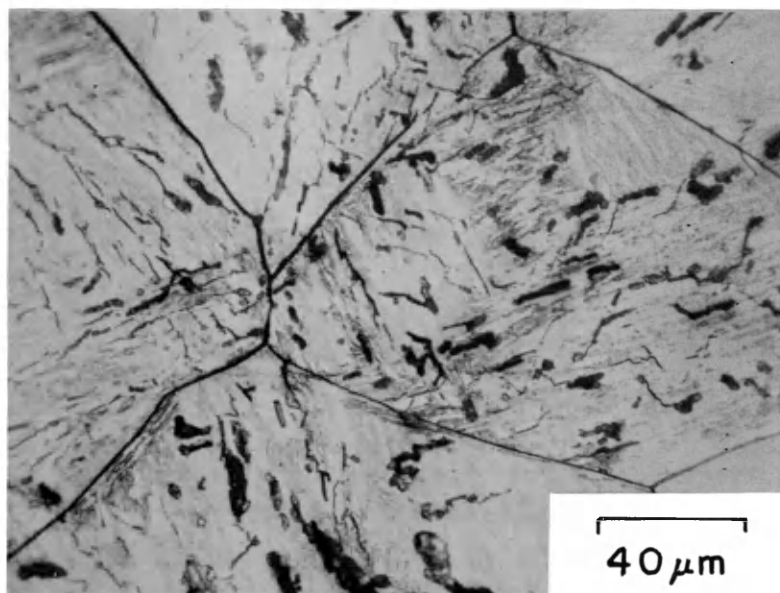
1. Initial Corrosion: The lithium primarily follows prior austenitic grain boundaries but branches off and directly attacks matrix precipitates. Micrographs of penetration during initial corrosion are shown in Figure 22. The depth of the attack of the coupon in Figure 22 actually extends 0.3 mm below the field of view of Figure 22a. The dark spots within grains in Figure 22 are areas of lithium attack where carbides previously existed. Figure 22 suggest that lithium follows a path set down by  $\epsilon$ -carbide plates. The lithium appears to have a higher mobility on grain boundaries.

Although  $\epsilon$ -carbide is generally thought to precipitate within ferrite laths(44) Baker and Nutting(37) observed  $\epsilon$ -carbide precipitation at grain boundaries after tempering for short times at 400C. The presence of  $\epsilon$ -carbide at grain boundaries is consistent with the appearance of the attack in Figure 22.

The initial corrosion rate is not a strong function of temperature. One explanation for the low activation energy might be that the reaction is controlled by liquid-state diffusion. Bates(7) obtained values of 6.5 and 10 kcal/mole for the liquid diffusion controlled nickel leaching of an iron-nickel superalloy by lithium. Other investigators have obtained similar low values of activation



(a)



(b)

Figure 22: Corrosion of a simulated weldment during the initial corrosion mechanism. Exposure: 191 hrs in Li-17.6% Pb at 400C ((a)&(b) are the same coupon at different magnifications.)

energy for diffusion in liquid metals(45).

A schematic of the proposed model for the initial corrosion is shown in Figure 23. Carbon saturated lithium reacts with grain boundary and matrix carbides and  $\text{Li}_2\text{C}_2$  precipitates. Since the lithium behind the corrosion front is not saturated with carbon, the lithium carbide dissolves and carbon diffuses through the corroded grain boundary to the carbon-deficient lithium in the bath. This diffusion of carbon through the lithium in the grain boundary is most likely the rate controlling step in the initial corrosion of this material.

Figure 18 shows that austenitizing temperature affects the initial corrosion rate of simulated weldments. If we are correct in assuming that this corrosion is liquid diffusion controlled, a low austenitizing temperature must somehow affect the material so as to inhibit carbon diffusion in the lithium. Prior austenitic grain size, which is a strong function of austenitizing temperature, might affect the kinetics of carbon diffusion through corroded grain boundaries. Grain boundary corrosion produces a network of channels in the steel. Diffusion through these channels would be similar to diffusion of a fluid through a compacted bed of solid particles. The effective diffusivity is inversely proportional to the

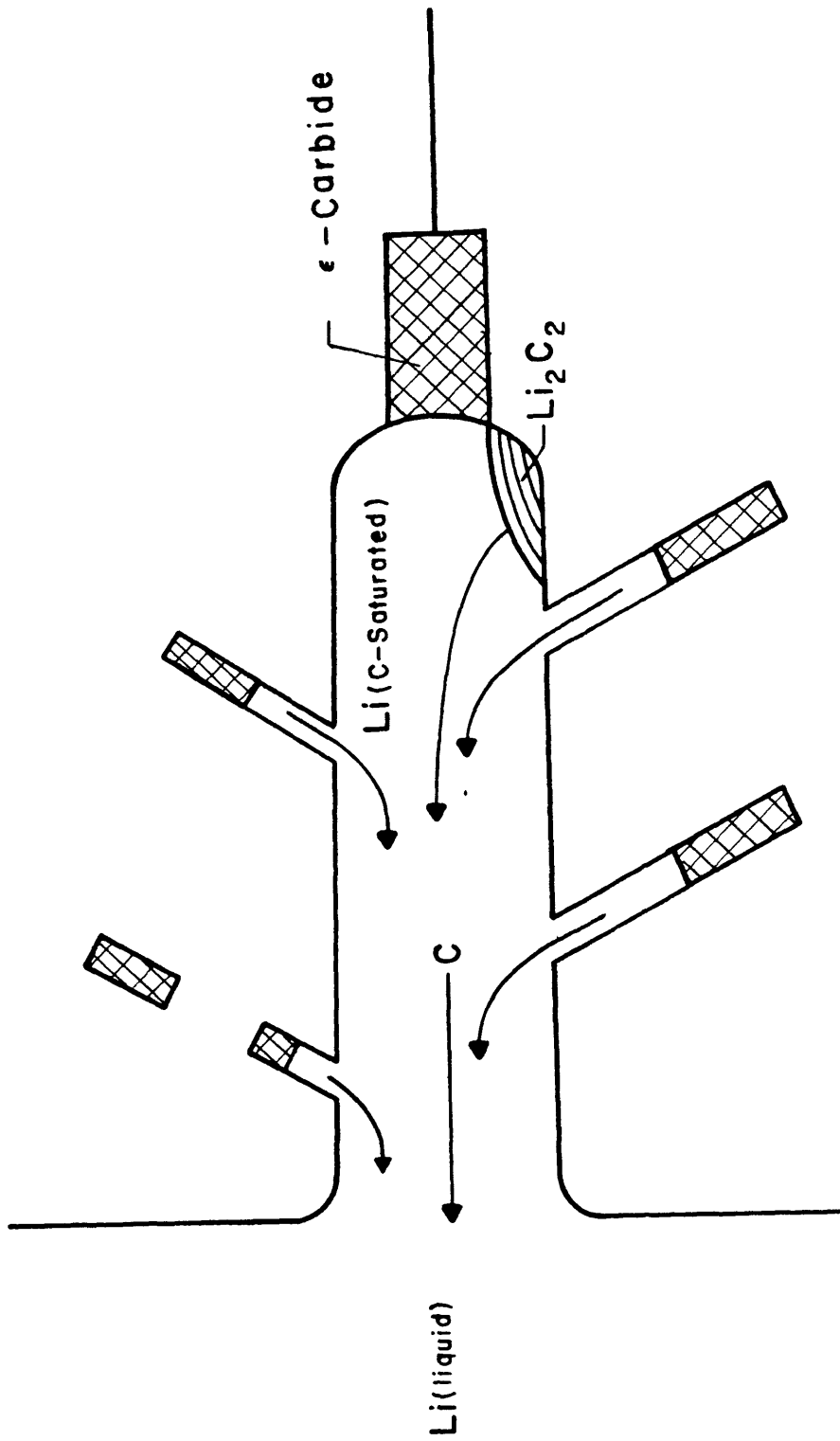


Figure 23: Schematic of a corroded grain boundary during the initial corrosion mechanism. Lithium converts epsilon carbide to  $\text{Li}_2\text{C}_2$  which dissolves in the lithium. The reaction is controlled by the rate of carbon diffusion through the corroded grain boundary.

tortuosity(45). Tortuosity is a function of particle size and shape. A material with a small grain size would have a high tortuosity and therefore a low diffusivity in the corroded grain boundary network. The average grain diameter produced by the 1300C austenitizing treatment is approximately 150 microns while the 927C heat treatment produced a grain size of only ~10 microns.

2. Secondary Corrosion: The appearance of the corrosion after the formation of cementite is slightly different than the initial corrosion as shown in Figure 22. Figures 24&25 are micrographs which show the typical appearance of secondary corrosion. Figure 25 compares the uncorroded microstructure with the matrix surrounding a corroded grain boundary. Note that during secondary corrosion the lithium attacks only the grain boundaries. The grains surrounding the corroded boundaries are decarburized because lithium has an affinity for carbon(14,32).

As  $\epsilon$ -carbide is transformed to cementite the grain boundary carbides thicken(37). Cementite is more stable than  $\epsilon$ -carbide; hence the dissolution of cementite is probably slower. The activation energy of 28 kcal/mole most likely corresponds to a reaction controlled mechanism because it is too high for liquid diffusion or for carbon diffusion in ferrite (which has an activation energy of

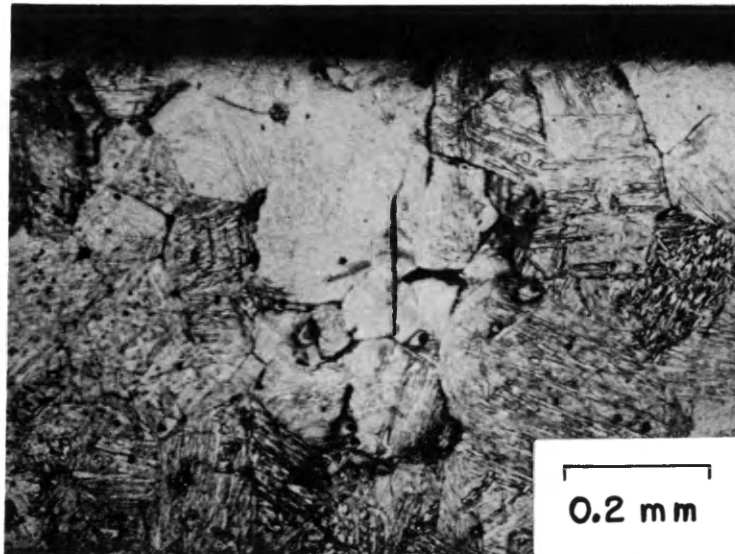
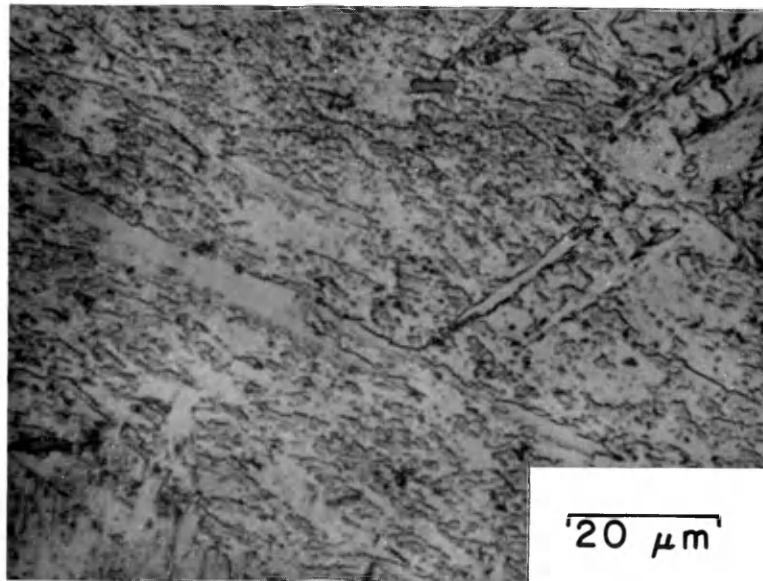
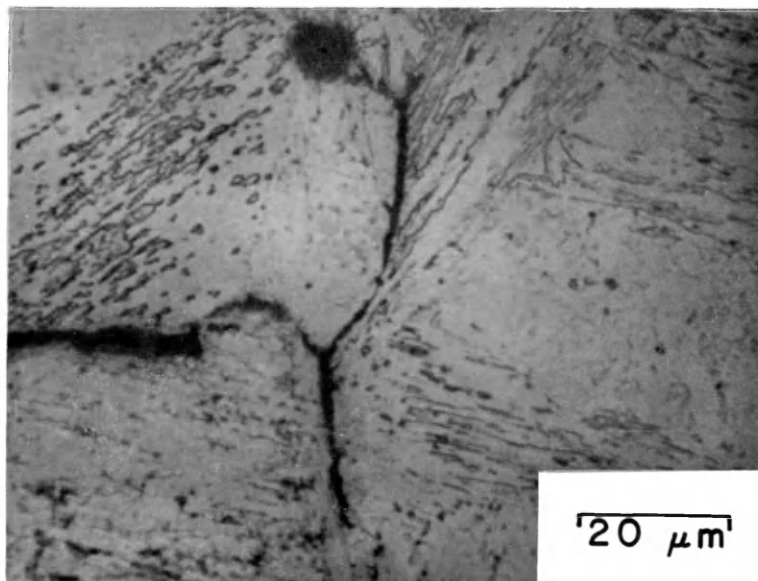


Figure 24: Decarburization of a simulated weldment  
(oil quenched from 1300C) during secondary  
corrosion.  
Exposure: 63 hrs in Li-17.6% Pb at 580C



(a) Uncorroded matrix



(b) Decarburized matrix

Figure 25: Comparison of the uncorroded microstructure and the matrix decarburized during secondary corrosion.  
Exposure: 63 hrs in Li-17.6% Pb at 500C

about 18 kcal/mole).

A schematic of the proposed corrosion model is shown in Figure 26. The penetration rate is controlled by the rate of dissolution of grain boundary cementite. Lithium carbide precipitates and dissolves as carbon diffuses out of the grain boundary. The lithium in the boundary acts as a carbon sink as it decarburizes the matrix (Figures 24&25). This decarburization is probably a parallel reaction and therefore does not affect the penetration rate.

#### Auger Spectroscopy

A GTA-welded coupon of 2 1/4 Cr - 1 Mo steel exposed to lithium (no lead) for 240 hours at 500C was fractured in a  $10^{-9}$  Torr vacuum. The sample was fractured in the heat-affected zone where intergranular attack had occurred, and the fracture surface was analyzed by Auger spectroscopy.

Figure 27 shows the Auger spectra from three regions on the fracture surface. High concentrations of sulfur and oxygen were found at the prior austenitic grain boundaries, even in grain boundaries not yet reached by the lithium. Apparently, the sulfur segregation to the grain boundaries is a result of the temperature gradients imposed by the welding process. It is not known what role, if any, the sulfur and oxygen play in the corrosion of this steel by

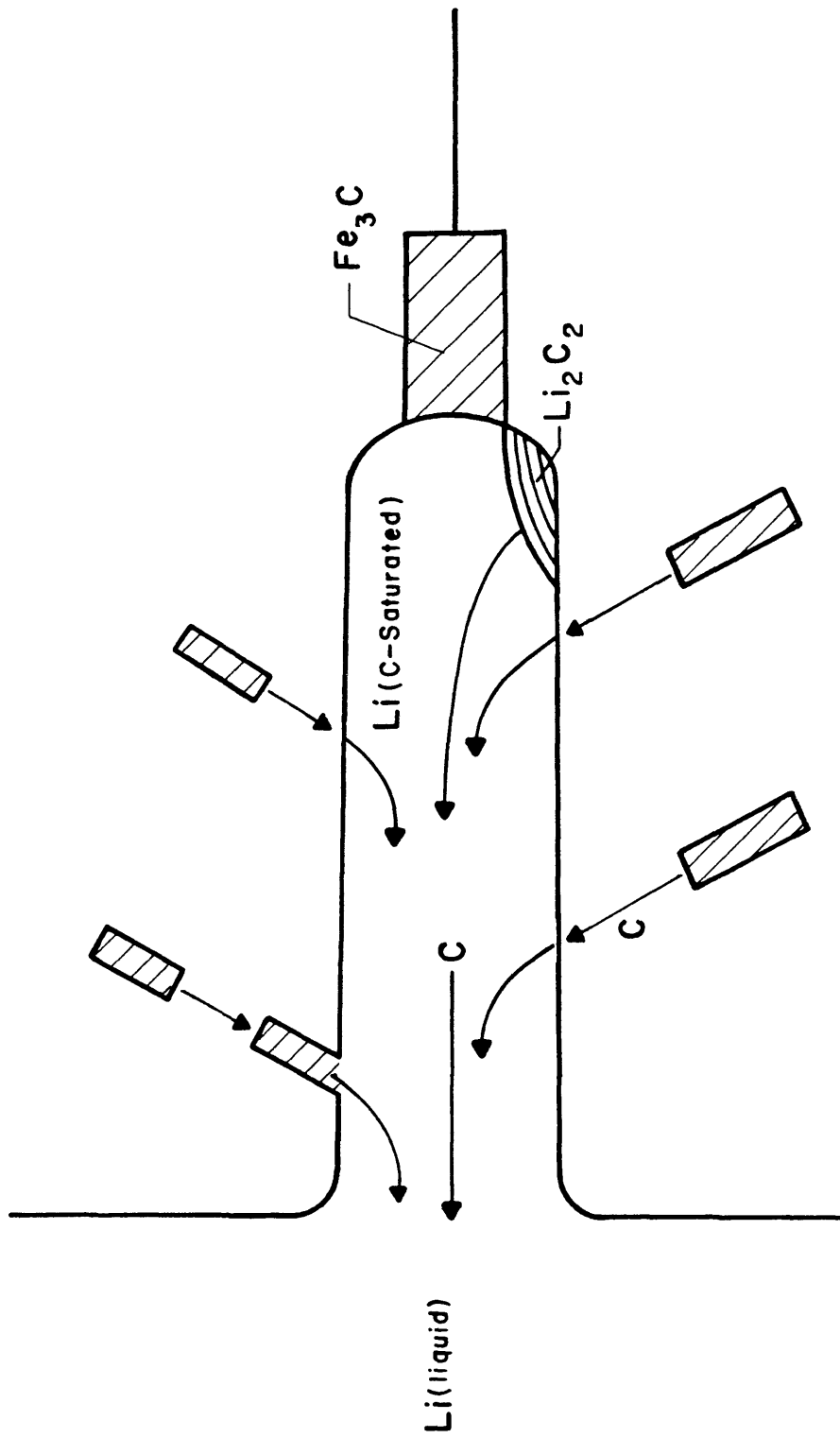


Figure 26: Schematic of a corroded grain boundary during the secondary corrosion mechanism. The reaction is controlled by the rate of dissolution of cementite.

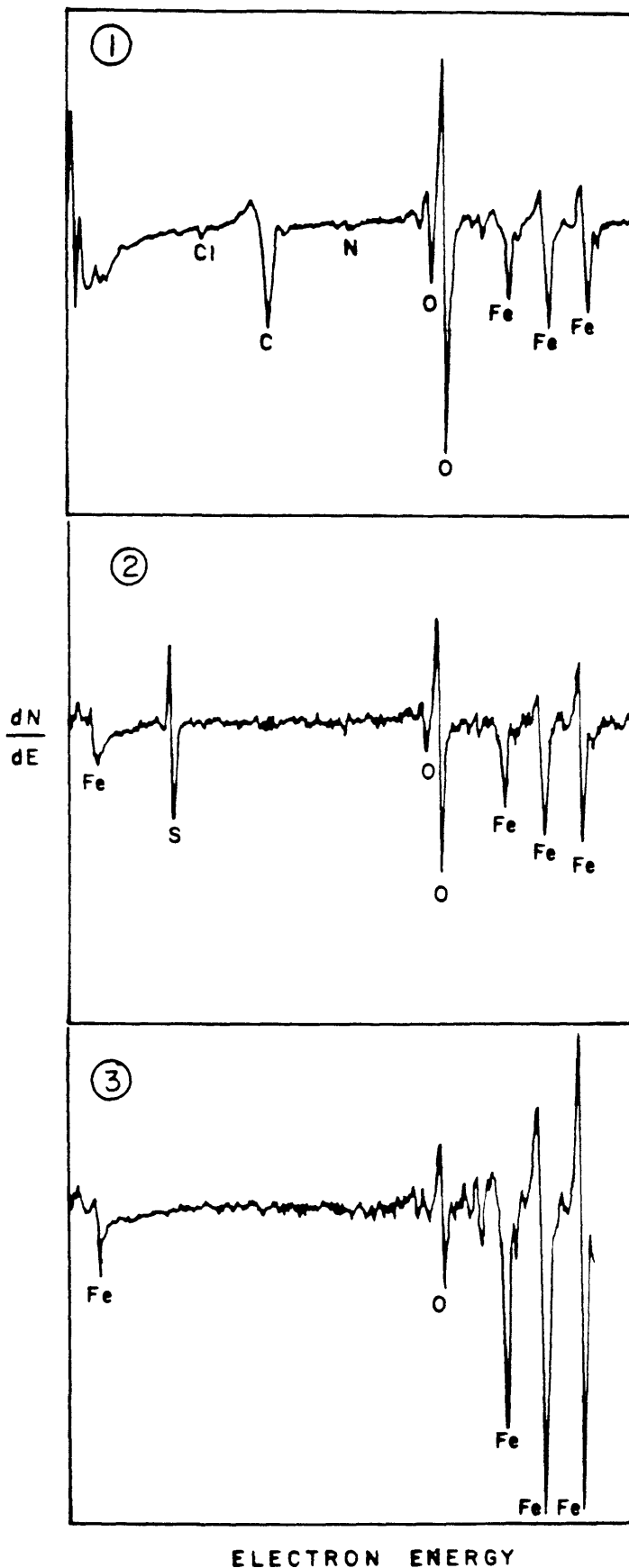
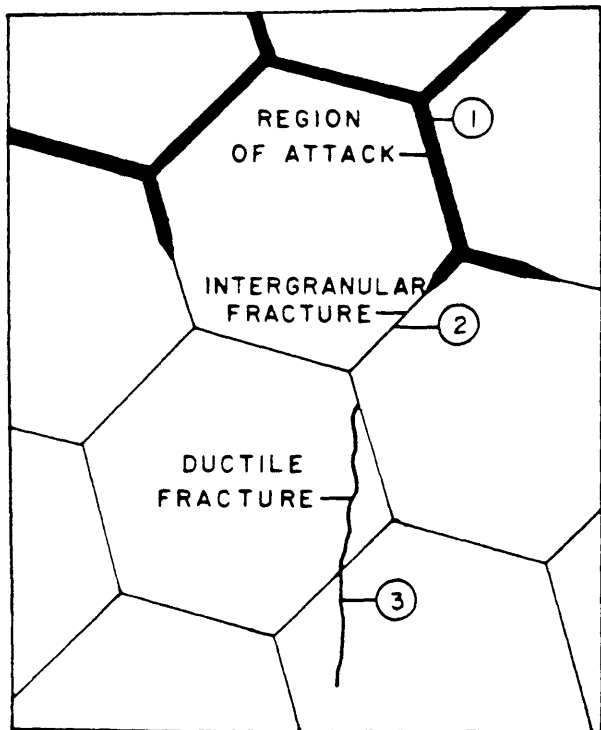


Figure 27: Auger spectra of three regions of a GTA weldment fractured along a corroded grain boundary. The specimen was exposed to lithium (no lead) at 500C for 240 hrs.

lithium.

Schowengert and Forrest(47) performed Auger spectroscopy on simulated weldments exposed to lithium at 500C. They attempted to identify lithium corrosion products by analyzing the low energy end of the spectrum by means of the second derivative of intensity. No lithium carbide corrosion product was observed; however, lithium oxide was seen at corroded grain boundaries.

$\text{Li}_2\text{C}_2$  can be converted to  $\text{Li}_2\text{O}$  in the presence of oxygen. It is possible that lithium carbide decomposed to form lithium oxide when the corroded grain boundaries were exposed to air when the sample was removed from the glove box.

#### Weight Loss

Coupons with a known surface area were weighed before and after exposure to lithium-lead. The weight loss of both regular grade and Nb-stabilized 2 1/4 Cr - 1Mo steel in low nitrogen (~50 ppm) lithium - 17.6 weight percent lead was negligible (< 0.2 mg/cm after 1600 hours exposure at 500C). Meaningful data from these weight loss tests could not be collected because the measured values of weight loss were of the same order of magnitude as the maximum sensitivity of the analytical balance.

Previous data(1) showed that measurable weight loss of 2 1/4 Cr - 1 Mo steel occurred in lithium containing ~500 ppm nitrogen. The rate of dissolution was accelerated when the nitrogen content increased to 2500 ppm.

Apparently weight loss will not be a significant problem in lithium loops, as long as the nitrogen level is maintained at a low value (<100 ppm). However, these tests were performed in static lithium. It remains to be seen what effect the velocity of lithium will have on the dissolution rate of the steel.

#### Stress Effect

Figure 11 shows that an applied stress of 18 ksi has little or no effect on the rate of intergranular penetration in the HAZ of a GTA weldment. Several tensile specimens which were given weld-simulating heat treatments were loaded to a maximum stress of 40 ksi in lithium-lead at 500C. The samples had variable cross sections which produced a range of stresses in each sample when a load was applied. Nominal stresses in a given sample ranged from 20 to 40 ksi. Two of these samples fractured intergranularly immediately upon application of the load. A third sample sustained the load for the entire duration of the test (100 hrs.) without fracturing. When this specimen was sectioned and examined

metallographically, it was found that the applied stress did not measurably accelerate the penetration.

Whipple, et. al.(13) showed a direct correlation between creep rate and penetration rate in Armco iron. Since the creep rate in 2 1/4 Cr - 1 Mo is negligible at 40 ksi at 500C, it is reasonable to expect a negligible stress contribution to the corrosion rate under these conditions. The simulated HAZ structure is fairly brittle. It is possible that some of the tensile samples had small, undetectable flaws which produced a stress concentration which was sufficient for fracture.

The results of these stress tests are not well understood. A complete experimental analysis with a more systematic approach is needed for a better understanding of stress-corrosion relationships.

SUMMARY AND CONCLUSIONS

GTA weldments of 2 1/4 Cr - 1 Mo steel are susceptible to severe intergranular attack in the heat-affected zone by lithium-17.6 weight percent lead because the cementite and epsilon carbide in the HAZ are thermodynamically unstable in lithium below ~700C. Corrosion resistance of 2 1/4 Cr - 1 Mo weldments can be greatly improved by a post-weld heat treatment which converts the unstable carbides to carbides which are stable in lithium such as  $M_{23}C_6$ . An insufficient post-weld temper will produce needle-like  $Mo_2C$  precipitates which are susceptible to lithium attack. Niobium-stabilized 2 1/4 Cr - 1 Mo steel forms stable, refractory carbides upon cooling from from the austenitic range; a post-weld heat treatment is not required for corrosion resistance.

The heat-affected zones of GTA weldments can be adequately simulated by an appropriate heat treatment. This material (along with an actual GTA HAZ) corrodes at an initially high rate. This rate has an activation energy of 5.3 kcal/mole and is probably controlled by the rate of carbon diffusion through the lithium in the grain boundary. When epsilon carbide is converted to cementite upon tempering in the lithium, the penetration rate is reduced. The secondary penetration rate, which has an activation

energy of 28 kcal/mole, is most likely reaction controlled rather than diffusion controlled.

The corrosion rate is not a strong function of cooling rate from the austenitic range; but the initial corrosion rate increases with increasing austenitizing temperature. It is believed that the larger grain size produced at a higher austenitizing temperature speeds the corrosion by providing an easier diffusion path for carbon through the corroded grain boundary.

High concentrations of sulfur and oxygen at corrosion-susceptible grain boundaries of 2 1/4 Cr - 1 Mo steel, and lithium oxide has been found at corroded grain boundaries. The role of oxygen and sulfur at corrosion-susceptible grain boundaries is not currently known; however the presence of lithium oxide as a corrosion product is consistent with the proposed mechanisms of corrosion.

REFERENCES

1. Edwards, G. R. and Olson, D. L., Liquid Lithium Corrosion Screening Tests for Hylife, 1978 Annual Report, LLL, Colorado School of Mines, October 1978.
2. Hoffman, E. E., Corrosion of Materials by Lithium at Elevated Temperatures, ORNL 2924, 1960.
3. Wilkinson, W. D. and Yagee, F. L., Attack on Metals by Lithium, ANL 4990, 1950.
4. Cunningham, J. E., Resistance of Metallic Materials in Corrosion Attack by High-Temperature Lithium, ORNL-CF-51-7-135, 1951.
5. Brasunas, A., Interim Report on Static Liquid-Metal Corrosion, ORNL 1647, 1954.
6. Olson, D. L. and Bradley, W. L., The Corrosion of Ferrous Alloys in Nitrogen-Contaminated Liquid Lithium, ERDA Conference Report CONF-760503-P1, pp. 446-452, 1976.
7. Bates, D. A., Master of Science Thesis, Colorado School of Mines, T-2092, 1978.
8. Hoffman, E. E. and Manly, W. D., Advances in Chemistry, Am. Chem. Soc., Series 19, pp. 82-92, 1957.
9. Manly, W. D., Corrosion, 12, p. 336, 1956.
10. Weeks, J. R. and Klamut, C. J., Liquid-Metal Corrosion Mechanisms, Corrosion of Reactor Materials I, International Atomic Energy Agency, Vienna, 1962.
11. Popovich, V., Goickham, M. s., Datishin, A. M., Toropovskaya, I. N., Shytkaylo, I. G. and Chaevskii, M. I., Fiz. Khim. Mikh. Mat., 3, pp. 24-32, 1967.
12. Jordan, W., Bradley, W. L., and Olson, D. L., Nucl. Tech., 29, pp. 209-214, 1976.
13. Whipple, T. A., Master of Science thesis, Colorado School of Mines, T-1916, 1976.
14. Beskorovainyi, N. M., Ivanov, V. K., and Zuev, M. T., Behavior of C in Systems of the Metal-Molten Metal-C Type,

- High Purity Metals and Alloys-Fabrication, Properties and Testing No. 5 Atomizdat, Moscow, 1966, Eng. Translation by Consultants Bureau, pp. 107-119, 1967.
15. Selle, J. E., Corrosion of Iron Base Alloys by Lithium, ERDA Conference Report CONF-760503-P2, pp. 455-461, 1976.
  16. Devan, J. H., Selle, J. E., and Morris, A. E., Review of Lithium Iron-Base Alloy Corrosion Studies, ORNL/TM 4927, 1976.
  17. Bunker, C. E., Test Results of Li Mass Transfer Loop LDL-1, Report TIM-405, 1957.
  18. Seebold, R. E., Corrosion, 16, p. 468, 1960.
  19. Boyer, M. H., Information of the Resistance of Materials to Attack by Molten Lithium, Report CRD-T2C-33, 1951.
  20. Klodney, M. and Minushkin, B., A Method for Determining the Solution Rate of Container Metals in Lithium, Report NDA-41, 1951.
  21. Gorkham, M. S. and Chavskii, M. T., Fiz. Khim. Mekh. Mat., 6, pp. 106-108. 1970.
  22. Reser, G. N., Predicting the Controlling Mode in the Corrosion of 304L Stainless Steel by Liquid Lithium, M. S. Thesis, Colorado School of Mines, T-2019, 1977.
  23. Schlager, R. J., Olson, D. L., and Bradley, W. L., Nucl. Tech., 27, pp. 439-441, 1975.
  24. Patterson, R. A., Schlager, R. J., and Olson, D. L., J. Nucl. Mat., 57, pp. 312-316, 1975.
  25. Dana, A. W., Baker, O. H., Fergeson, M., Investigation of Metal Transport by Liquid Lithium, Tech. Rept. V, B & W-5320, DC-52-27-45, 1952.
  26. Elrod, H. G., Fouse, R. R., and Richards, P. B., Erosion and Heat Transfer with Molten Lithium, Final Report, Rept. NEPA 1837, B & W Rept. 5217, 1951.
  27. Leavenworth, H. W. and Cleary, R. E., Acta Met., 9, p. 519, 1961.

28. Dmukhovskaya, I. G., Shatinskii, V. F., and Sinelnikova, O. G., *Zaschita Metallov*, 11, pp. 21-26, 1975.
29. Goikhman, M. S., *Fiz. Khim. Mat.*, 6, pp. 107-109, 1970.
30. Katsuta, H. and Furukawa, J., *J. of Nuc. Mat.*, 71, pp. 95-104, 1977.
31. Demastry, J. A., *Nuc. Appl.*, 3, pp. 127-134, 1967.
32. Beskorovainyi, N. M. and Ivanov, V. K., *High Purity Metals/Alloys Fabrication, Properties and Testing*, pp. 121-129.
33. Matlock, D. K., Spencer, R. E., Hammon, D. L., Whipple, T. A. and Olson, D. L., *Interrelationship Between Corrosion and Deformation Processes of Materials in Liquid Lithium*, Second International Conference on Liquid Metal Technology in Energy Production, Richland, WA, April 20-24, 1980.
34. Brehm, W. F., Gregg, J. L., Che Yu Li, *Trans. AIME*, 242, pp. 1205-1210, 1968.
35. Lautzenheiser, C. E., *Use of Quenched and Tempered 2 1/4 Cr - 1 Mo Steel*, Climax Molybdenum Co., New York, May 1965.
36. Lai, G. Y., *On the Precipitation of Epsilon Carbide in Lower Bainite*, *Met. Trans.*, vol. 6A, July 1975, pp. 1469-1471.
37. Baker, R. G. and Nutting, J., *The Tempering of 2 1/4 Cr - 1 Mo Steel After Quenching and Normalizing*, *J. Iron and Steel Inst.*, 192, No. 7, p. 257, 1959.
38. Habrahen, L. J. and Economopoulos, M., *Transformations and Hardenability in Steels Symposium*, Climax Molybdenum Co. and the University of Michigan, 1967, p. 71.
39. Copeland, J. F. and Pense, A. W., *Hardenability: Key to Vessel Plate Strength*, *Hydrocarbon Processing*, April 1974.
40. Leitnaker, J. M., Kluehn, R. L., and Lang, W. R., *Met Trans.*, 6A, p, 1949, 1975.
41. Alberry, P. J. and Jones, W.K.C., *Metals Technology* pp. 360-364, 1977.

42. Smith, E. and Nutting, J., JISI, 1957, vol. 187, pp. 314-329.
43. Wilkinson, B., unpublished work, Colorado School of Mines, 1980.
44. Jack, K. H., JISI, 1951, vol. 169, pp. 26-36.
45. Walls, H. A., Techniques in Metals Research, vol IV, 1968.
46. Gieger, G. H. and Poirier, D. R., Transport Phenomena in Metallurgy, Addison-Wesley, Reading, MA, 1977.
47. Schowengert, F. D. and Forrest, J. S., Auger Spectra of Lithium Compounds, Second International Conference on Liquid Metal Technology in Energy Production, Richland, WA, April 20-24, 1980.